Electronic Supplementary Material (ESI) for New Journal of Chemistry.

Supporting Information

Gelation-induced enhanced emission active stimuli-responsive low-molecular-weight organogelator: Dual-channel recognition of cyanide from water and food samples with superhydrophobic surface formation

Kingshuk Debsharma,[*,a] Sunanda Dey,[b,c] Jyothibabu Sajila Arya,[a] Krishna Sundar Das,[d]

Chittaranjan Sinha,[b] Edamana Prasad[*,a]

[a]Department of Chemistry, Indian Institute of Technology Madras (IIT M), Chennai 600 036,

India

[b]Department of Chemistry, Jadavpur University (JU), Kolkata 700032, India

[c]Department of Chemistry, Mrinalini Datta Mahavidyapith, Birati, Kolkata 700051, India

[d]Indian Association for the Cultivation of Science (IACS), Kolkata, 700032, India

Corresponding Authors' Email Address: ju34kingshukdbs@gmail.com;

cy16d041@smail.iitm.ac.in

Experimental Methods

Synthesis and Characterization of CN1

CN1 was synthesized based on a reported single step knoevenagel condensation reaction.[1,2] To an ethanolic solution of 4-nitrophenylacetonitrile (1.69 g, 0.01 mol), was added triethylamine (1.6 mL, 0.02 mol) and pyrene-1-carboxaldehyde (2 g, 8.69 mmol) followed by refluxing the resultant reaction mixture for 6 hours. The obtained precipitate was washed thoroughly with hot methanol for 5/6 times and the obtained residue was dried under high vacuum. Recrystallization the dried sample from DMF afforded a red colored solid CN1 (3.2 g, 98.47%). The formation of product was then confirmed and characterized completely from ^{1}H NMR and high resolution mass spectrometry (HRMS) techniques and the respective spectra were mentioned in Fig. S1 and Fig. S2. A Bruker 500 MHz spectrometer of Avance series and a micromass Q-TOF mass spectrometer were employed for NMR and HRMS techniques respectively. Tetramethylsilane [TMS; Si(CH$_3$)$_4$] was utilized as an internal standard in NMR measurement. Elemental analysis was performed with Perkin-Elmer (2400 Series-II, PerkinElmer, USA) CHN analyser. For ^{1}H NMR titration experiment with cyanide (CN$^-$), same instrumental facility was utilized. Owing to the limited solubility of CN1 in common organic solvents, characteristics ^{13}C NMR spectrum was not obtained after repeated trial. However, expected ^{13}C resonance signals were achieved after treating CN1 with CN$^-$ in a desired stoichiometric ratio under room temperature.

UV/Vis Absorption and Emission Studies

The solution and solid state UV/Vis absorption and emission characteristics of CN1 were carried out using a JASCO V-760 and Horiba Jobin Yvon Fluoromax-4 spectrophotometers respectively at room temperature. The quartz cuvettes having path length equalled to 1 cm with two and four faced transparent surfaces were utilized for UV/Vis absorption and emission studies of CN1 respectively in solution state. For the solid state and variable

temperature UV and PL studies, same instrumental facilities were employed with modified experimental accessories. For temperature dependent optical studies, DMF was used as a solvent medium owing to its lower freezing temperature. For monitoring gel phase PL feature a four phased transparent quartz having a path length equalled to 1 mm was used within the same instrumental setup. The respective spectral calibration plots, relevant to the analytical performance of CN1 were mentioned with error bars, which indicated standard error for the duplicate UV/Vis absorption and emission measurements.

Time Resolved Photoluminescence Decay Measurement

To inspect the time resolved photoluminescence behavior of CN1 in solution, solid and gel states a Horiba Jobin Yvon spectrometer with a diode laser source of 1 MHz pulse repetition rate was utilized in a time correlated single photon counting manner at room temperature. The respective emission maxima of the luminogen was monitored to record the time resolved fluorescence decay kinetics of CN1 based on following equation:

$$I(t) = \sum A_i e^{-\frac{t}{\tau_i}}$$

Where, τ_i and A_i represent lifetime component and its respective amplitude of the ith species.

To gather the lamp profile of the instrument, a colloidal solution of Ludox AS40, Sigma Aldirch was used in water. The respective decay profiles of the luminogen both in solution, solid and gel states were analysed by IBH DAS6 software with the recommended fitting range ($\chi^2 = 0.99 - 1.33$).

Absolute Fluorescence Quantum Yield Measurement

The absolute fluorescence quantum yields of CN1 in solution, solid and xerogel states were evaluated using a calibrated integrating sphere of steady state fluorescence spectroscopy based on the following equation[3]:

$$\phi = \frac{N_{em}}{N_{ab}} = \frac{\alpha \int \frac{\lambda}{hc} I_{em}(\lambda) d\lambda}{\alpha \int \frac{\lambda}{hc} [I_{ex}(\lambda) - I'_{ex}(\lambda)] d\lambda}$$

Where, N_{em}, N_{ab}, α, h and c are the emitted and absorbed photon numbers and the calibration factors for the measurement of Plank's constant and velocity of the light respectively. Corresponding intensity of emitted photons and intensities of excited laser beams in absence and presence of sample at λ are denoted by $I_{em}(\lambda)$, $I_{ex}(\lambda)$ and $I'_{ex}(\lambda)$ respectively.

Scanning Electron Microscopy (SEM)

To grasp the idea about surface topology of the developed xerogel from CN1 assembly, SEM microscopic techniques were employed as the imaging tools at room temperature. For these purposes a HITACHI S 4800 instrument was utilized on the properly diluted solution of the luminogenic aggregates on silica substrate after required drying the samples under high vacuum. Prior to SEM imaging a HITACHI E-1010 ion sputter was used for gold sputter coating the dried samples under room temperature.

Powder X-ray Diffraction (PXRD) Study

The packing arrangement of self-assemblies both in xerogel and solid states of CN1 were illustrated from the PXRD studies by utilizing a Bruker D8 Advance X-ray diffractometer under room temperature. Accordingly, a Cuk_{α} radiation, having a wavelength equaled to 1.54178 Å was used to diffract the samples.

Rheological Measurement

The structural stability of the developed self-assemblies was evaluated from the rheological measurements of CN1 organogel, which consider the variation in storage (G') and loss (G'') moduli with respect to the applied strain/stress and frequency in a desired oscillatory fashion during the amplitude and frequency sweep experiments respectively. An Antor Paar Compact Modular Rheometer (MCR 102) equipped with a well-controlled in-build PP25 system was utilized during the all rheological measurements under room temperature. Accordingly, the isothermal reversible gel-to-sol transition of CN1 assembly was monitored favourably from the time sweep thixotropic measurement during the alternative application of well-separated

low (0.01%) and high strains (30%) to affirm the complete conversion of gel-to-sol ($G' > G''$) and sol-to- gel ($G'' > G'$) under room temperature.[4,5]

The melting temperature (T_m) of the gel was determined from a temperature sweep experiment by monitoring the crossover of G' over G'' during desired variation in temperature under constant oscillatory stress/strain and frequency.

Water Contact Angle Measurement

A Holmarc model HO-IAD-Cam-01B instrument was utilized to determine the mean contact angles of CN1 coated glass slides and filter papers after appropriately placing the water droplet on the respective surfaces under room temperature.

Calculation of detection limits (DLs)

The detailed calculation for limit of detections (DLs) of CN1 towards CN⁻ both in solution [8:2 (v/v) DMSO/water] and gel state [8:2 (v/v) DMSO/water] were carried out based on following equation:

$$DL = 3\sigma/\mu$$

Where, σ is the standard deviation of absorbance and emission intensities of CN1 in solution as well gel in absence of CN⁻, which are tabulated below:

No	1	2	3	4	5	6	7	8	9	10
Intensity (a.u.)	0.19 543	0.19 545	0.19 575	0.19 595	0.19 620	0.19 623	0.19 634	0.19 637	0.19 650	0.19 641

Where, $\sigma = \sqrt{\sum(X_n - X_{avg})^2 / n}$ and $X_{avg} = 0.19606$

Accordingly, σ is calculated as 0.000397.

Similarly, for native CN1 gel the twelve emission intensities were tabulated below:

No	1	2	3	4	5	6	7	8	9	10	11	12
Intensity (a.u.)	542. 28	542. 03	542. 49	542. 45	542. 22	542. 62	542. 66	542. 83	542. 38	542. 70	542. 95	542. 71

Where, $\sigma = \sqrt{\sum(X_n - X_{avg})^2 / n}$ and $X_{avg} = 542.5267$

Accordingly, σ is calculated as 0.268272.

Now, μ denotes slope of the linear variation in absorbance and emission intensities of CN1 in presence of increased concentration of aqueous CN^- {$[CN^-]$} in micromolar regime (μM) both in solution [8:2 (v/v) DMSO/water] and gel [8:2 (v/v) DMSO/water]. Evidently the magnitudes of slopes were calculated as 0.2195 and 1.675 $μM^{-1}$ respectively. Henceforth, the DLs of CN1 for colorimetric and fluorogenic dual channel sensing towards CN^- were calculated as 5.42 nM and 0.48 μM respectively. For ascertain the accuracy, the absorption and emission spectral responses of gel towards CN^- were repeated to obtain the standard error for the sensing performance.

Computational Study

The energy minimized geometry of CN1 was optimized from b3lyp/6-311(+)g level of calculation from a Gaussian 09 suit of programme.[6] Correspondingly, the dimer structure of CN was simulated from molecular mechanics (MM+) calculation using hyperchem software.[7] The td-cam-b3lyp/cc-PVDZ level of theory was applied on the optimized geometry to elucidate the simulated absorption spectrum of CN1.

Preparation of cyanide-containing food samples for analytical measurements

To examine the capability of CN1 as a quantitative dual-channel cyanide sensor from food samples a detailed extraction procedure was followed prior examining the respective spectral disclosures of the receptor.[8,9] For this, the experimental food ingredients was kept in fresh water for 4 days and then minced carefully into the possible thinner shapes. The chopped samples were then crushed into pests and soaked in continuously stirred water overnight. The aqueous mixtures were then filtered and washed with water containing sodium hydroxide (100 mL, 100 mM) to obtain the cyanogenic solutions suitable for analytical experiments.
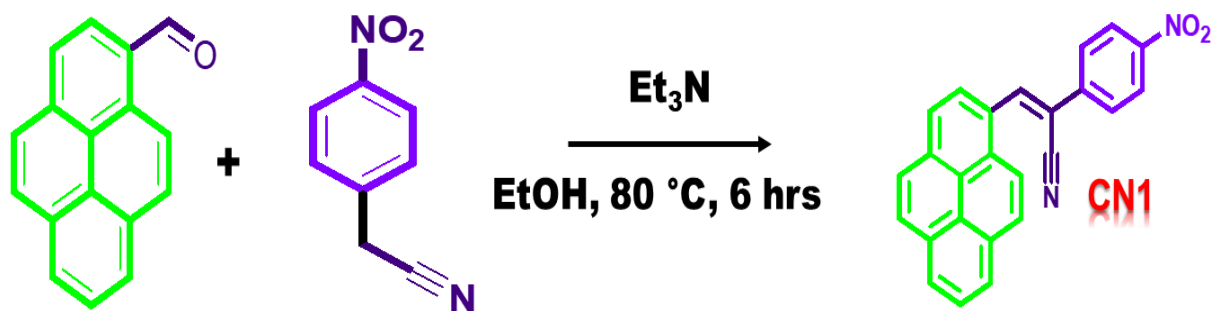
Scheme S1 Synthetic pathway for CN1.

Elemental analysis of $C_{25}H_{14}N_2O_2$ (CN1): calculated: C, 80.20; H, 3.77; N, 7.48; observed: C, 80.23; H, 3.73; N, 7.50.
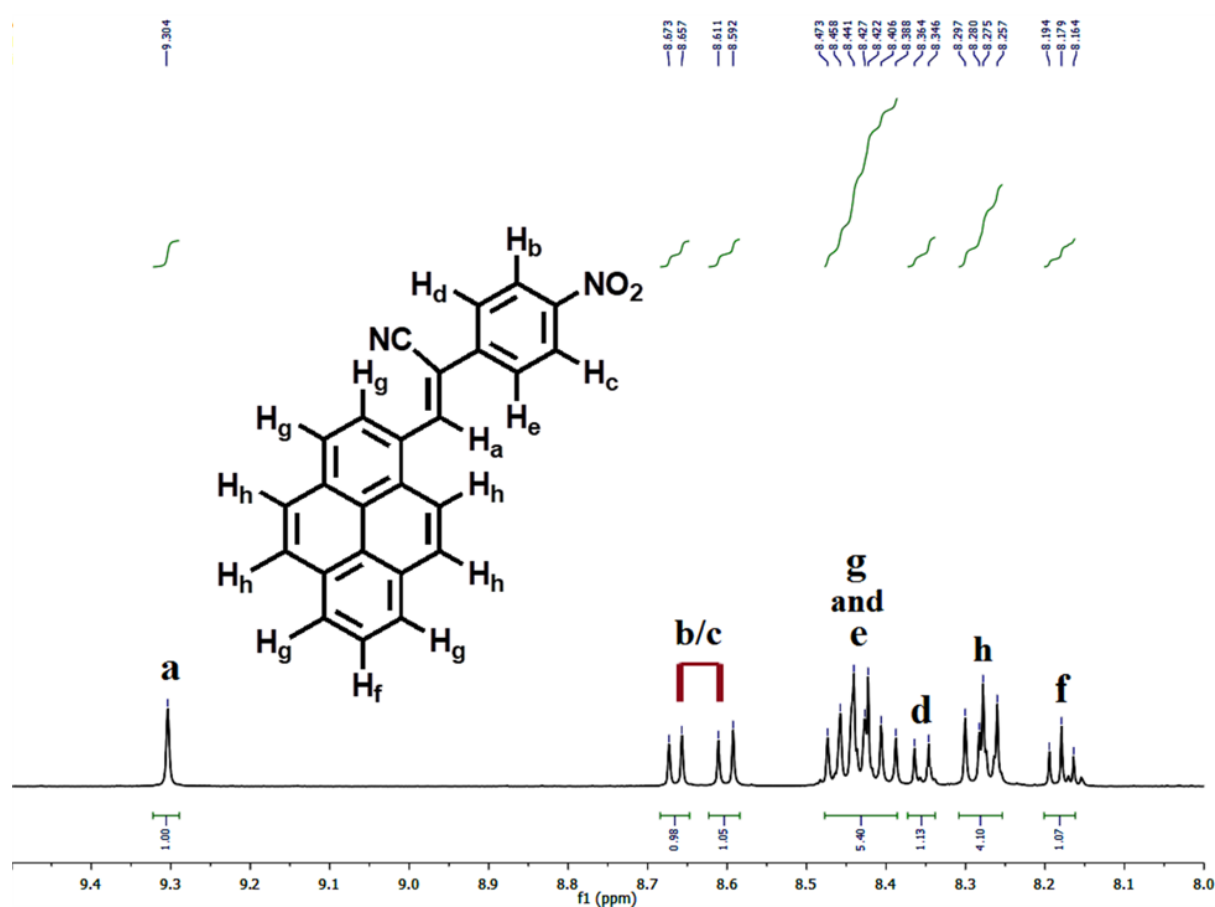
Fig. S1 ^{1}H NMR spectrum of CN1 in DMSO-d$_6$.

^{1}H NMR (500 MHz, DMSO-D$_6$): δ 9.30 (s, 1H), 8.67 (d, 1H), 8.61 (d, 1H), 8.38-8.47 (m, 5H), 8.36 (d, 1H), 8.25-8.29 (m, 4H), 8.19 (t, 1H).
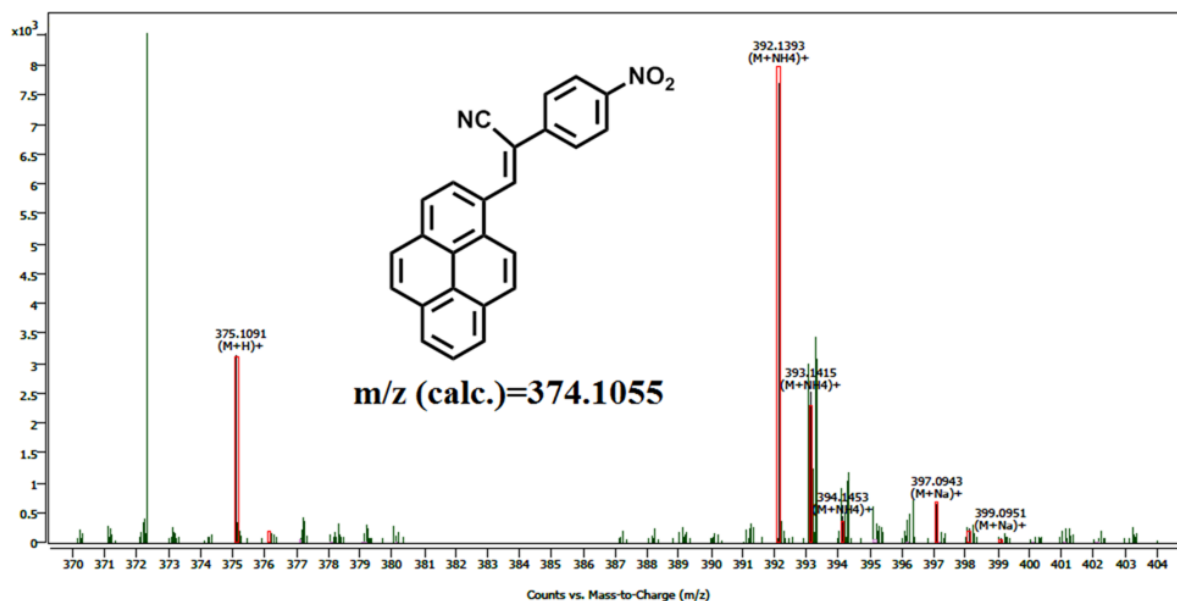
Fig. S2 HRMS plot of CN1.

Table S1 Gelation study of CN1 in different solvents and solvent mixtures. The critical gelation concentration (CGC) was indicated within parenthesis.

Solvents/solvent mixtures	CN1 (mg/mL)
Chloroform	I
Decanol	G (20)
1,4-dioxane	I
o-Dichlorobenzene	G (30)
Hexanol	I
Chlorobenzene	I
Xylene	I
Tetrachloroethylene	I
Dimethylformamide	G (15)
Dimethylsulphoxide	G (10)
Toluene	I
Ethyl acetate	I
Dichloromethane	I
Tetrahydrofuran	P
Hexane	I
Octanol	I
Acetone	I
1,2-Dichloroethane	I

Methanol	P
Acetonitrile	P
Mesitylene	G (15)
Anisole	G (20)
Dimethylformamide/Water (34:1)	G (20)
Dimethylsulphoxide/Water (8:2)	G (10)
Anisole/Methanol (15:1)	G (20)
Anisole/Hexane (15:1)	G (25)
Anisole/Chloroform (39:1)	PG (25)

G = gel; I = Insoluble; P = precipitation; PG = Partial gel
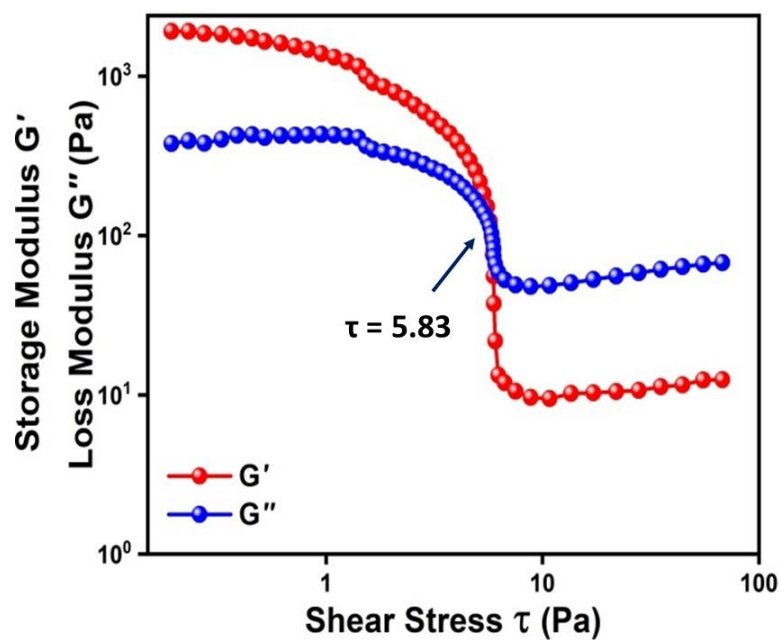
Fig. S3 Stress sweep experiment of CN1 gel obtained from DMSO (1 wt%).
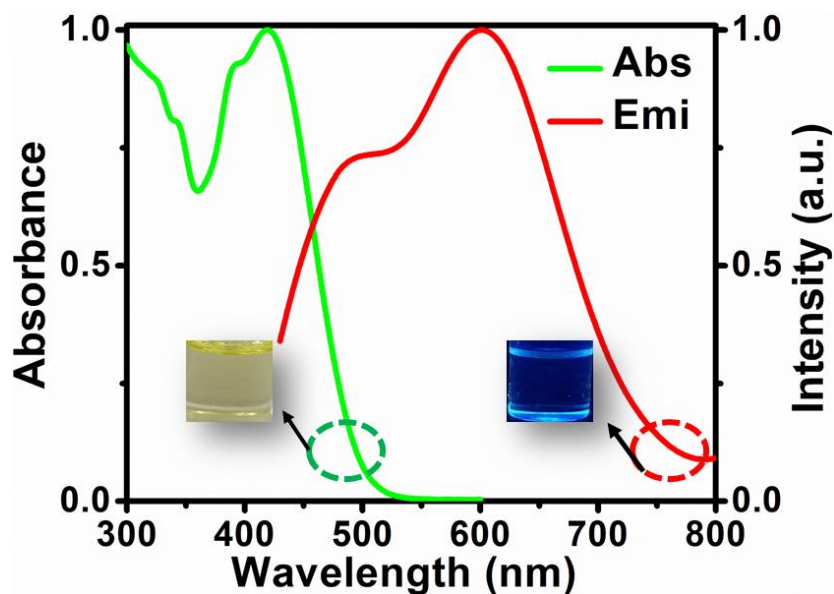
Fig. S4 Normalized absorption (left) and emission spectra (right) of CN1 in DMSO (concentration = 10 μM, λ_{ex} = 420 nm).
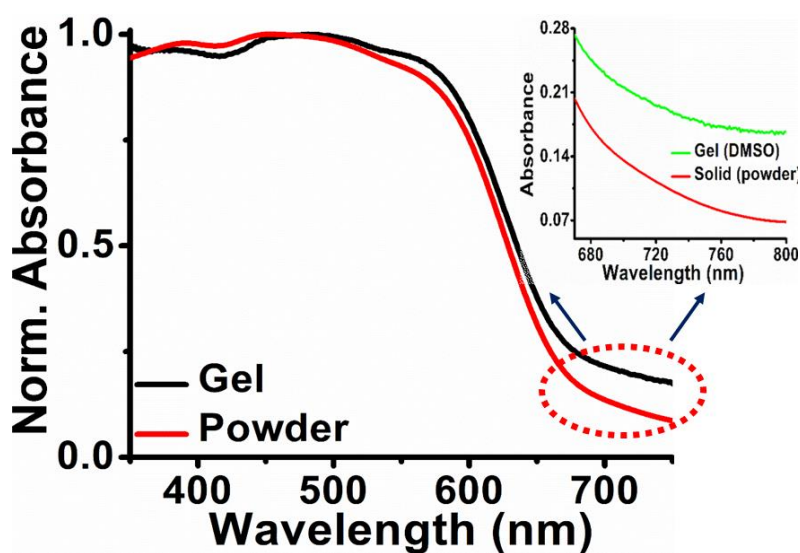
Fig. S5 UV/Vis absorption spectra of CN1 gel (DMSO, 1 wt%) and solid reveals respective tailing at higher wavelength region (Inset).
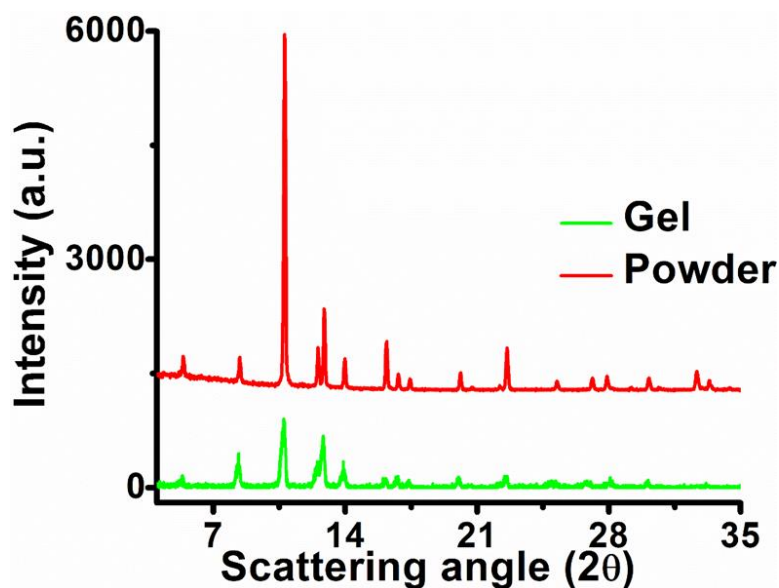
Fig. S6 PXRD patterns of DMSO gel (1 wt%) and as-synthesized powder of CN1.

Table S2 Analysis of PXRD profiles of DMSO gel (1 wt%) and as-synthesized powder of CN1.

CN1 gel ((DMSO, 1 wt%)		CN1 powder	
Scattering angle (2θ)	d_{hkl} (Å)	Scattering angle (2θ)	d_{hkl} (Å)
5.30	16.65 (d_{100})	5.39	16.39 (d_{100})
8.31	10.63 (d_{110})	8.39	10.54 (d_{110})
10.71	8.25 (d_{010})	10.78	8.21 (d_{010})
24.94	3.56 ($d_{\pi\cdots\pi}$)	25.25	3.52 ($d_{\pi\cdots\pi}$)
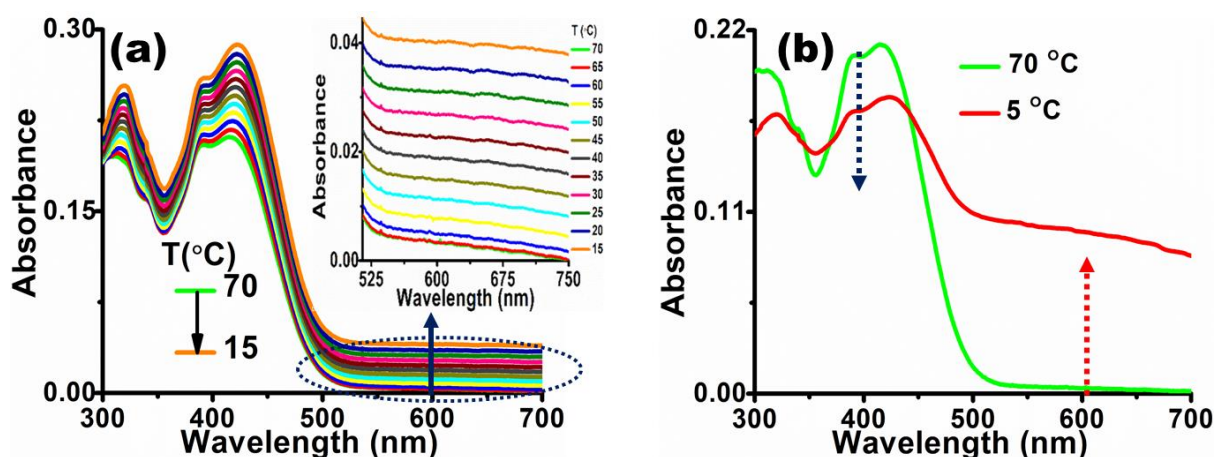
Fig. S7 (a) Variation in UV/Vis absorption spectra of CN1 (10 µM) in DMF represents intensified tailing at higher wavelength region with decreased temperature. (b) Broadening in UV/Vis absorption spectra of CN1 (10 µM) with tailing at higher wavelength region at lower temperature (5 °C) compared to that at higher temperature (70 °C).
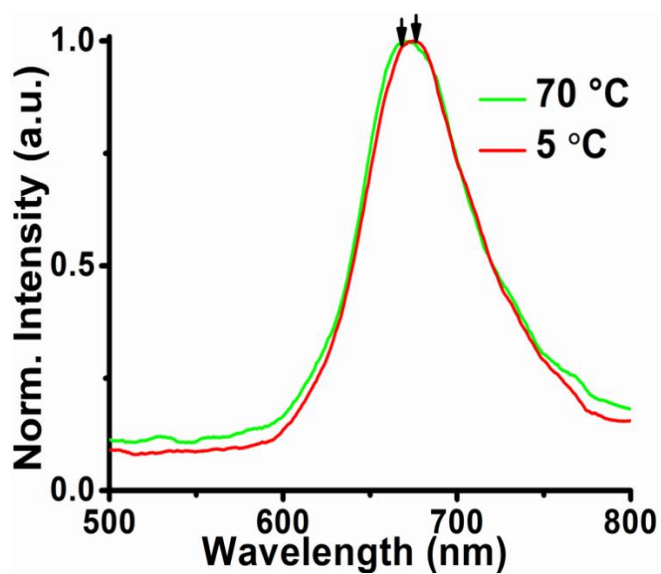
Fig. S8 Bathochromically shifted emission maxima of CN1 in DMF at 5 °C with respect to that at 70 °C. (Concentration = 10 μM, λ_{ex} = 420 nm).
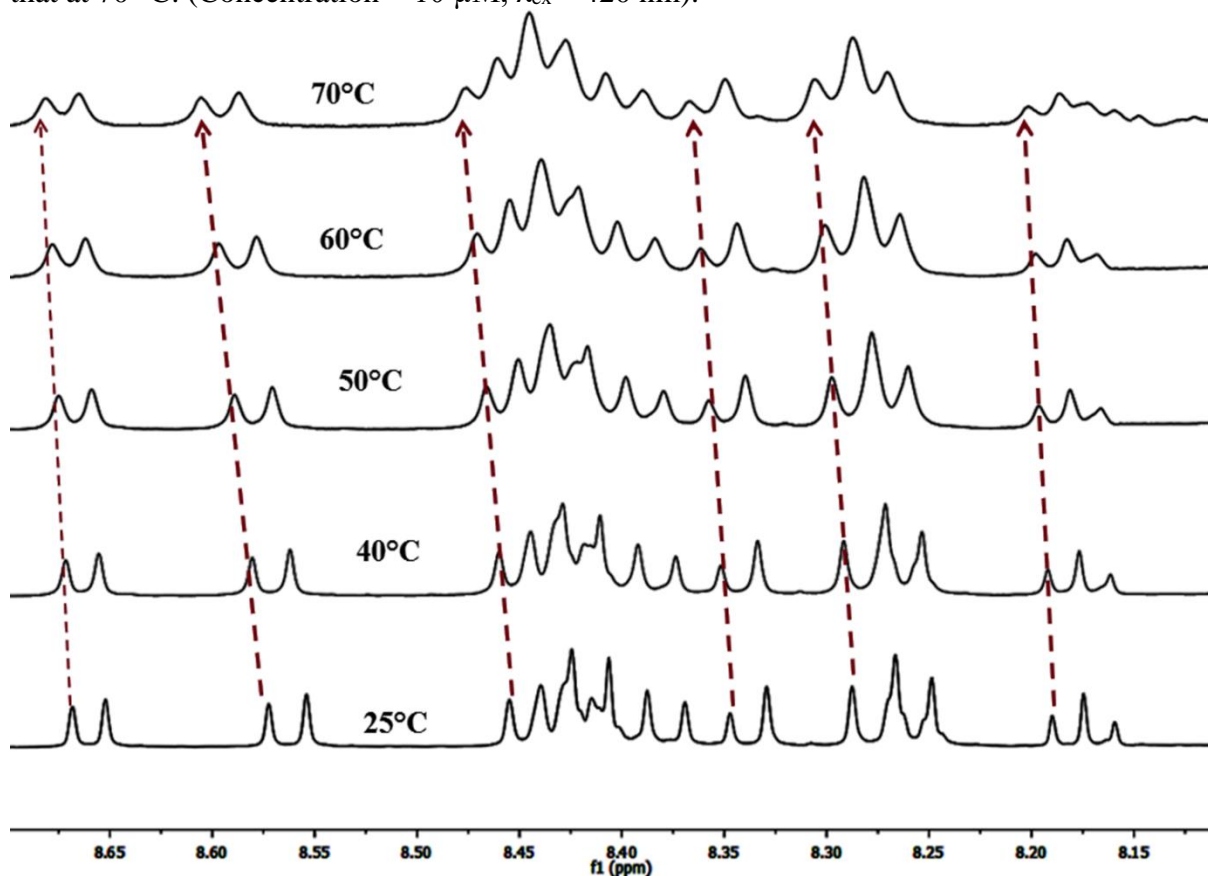
Fig. S9 Temperature dependent ^{1}H NMR profile of CN1 in DMSO-d_6 reveals conspicuous downfield shifting of all protons with increased temperature.

Table S3 Analysis of temperature dependent ^1H NMR of CN1

Temperature (°C)	H_b/H_c	H_g & H_e	H_d	H_h	H_f
25	8.673,8.657/8.611,8.592	8.388-8.473	8.364,8.346	8.257-8.297	8.194,8.179,8.164
40	8.676,8.660/8.619,8.601	8.393-8.478	8.369,8.351	8.262-8.302	8.197,8.183,8.167
50	8.680,8.664/8.628,8.609	8.399-8.484	8.374,8.357	8.267-8.308	8.200,8.186,8.171
60	8.683,8.667/8.635,8.618	8.404-8.489	8.379,8.362	8.272-8.313	8.203,8.189,8.175
70	8.686,8.670/8.644,8.626	8.410-8.494	8.384,8.367	8.276-8.319	8.207,8.192,8.178
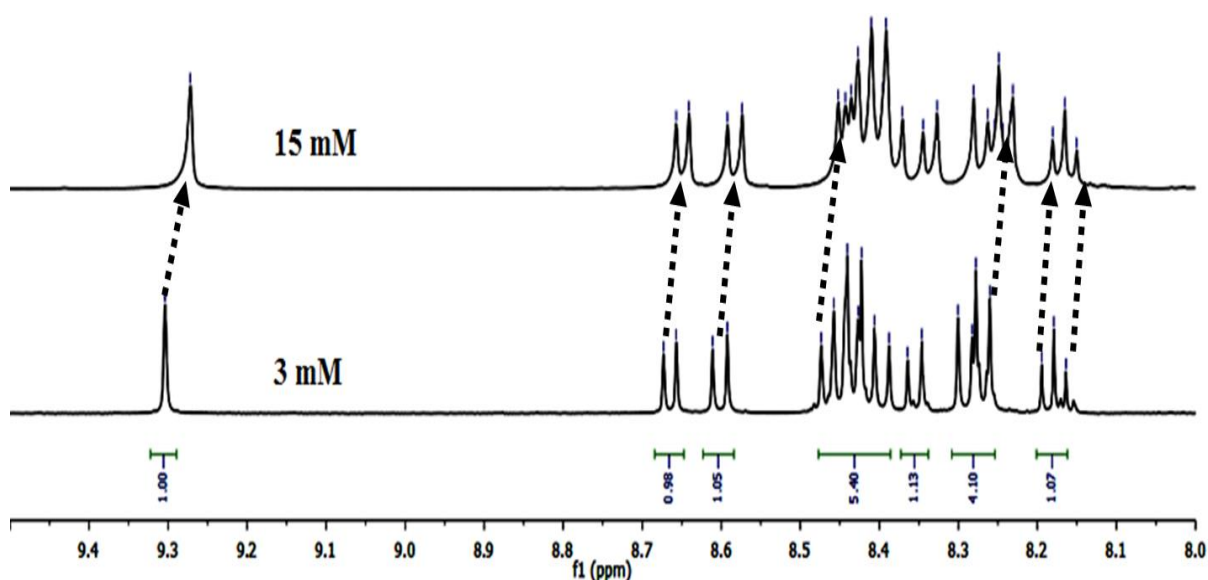
Fig. S10 Concentration dependent ^1H NMR profile of CN1 in DMSO-d_6 reveals conspicuous upfield shifting of protons at 15 mM compared to that at 3 mM.

Table S4 Analysis of concentration dependent ^1H NMR of CN1

Protons	3mM	6 mM	15 mM
H_a	9.304	9.297	9.271
H_b/H_c	8.673,8.657/8.611,8.592	8.669,8.653/8.607,8.568	8.656,8.640/8.591,8.573
H_g & H_e	8.388-8.473	8.384-8.469	8.370-8.451
H_d	8.364,8.346	8.360,8.342	8.344,8.326
H_h	8.257-8.297	8.263-8.302	8.231-8.280
H_f	8.194,8.179,8.164	8.191,8.176,8.161	8.180,8.165,8.150
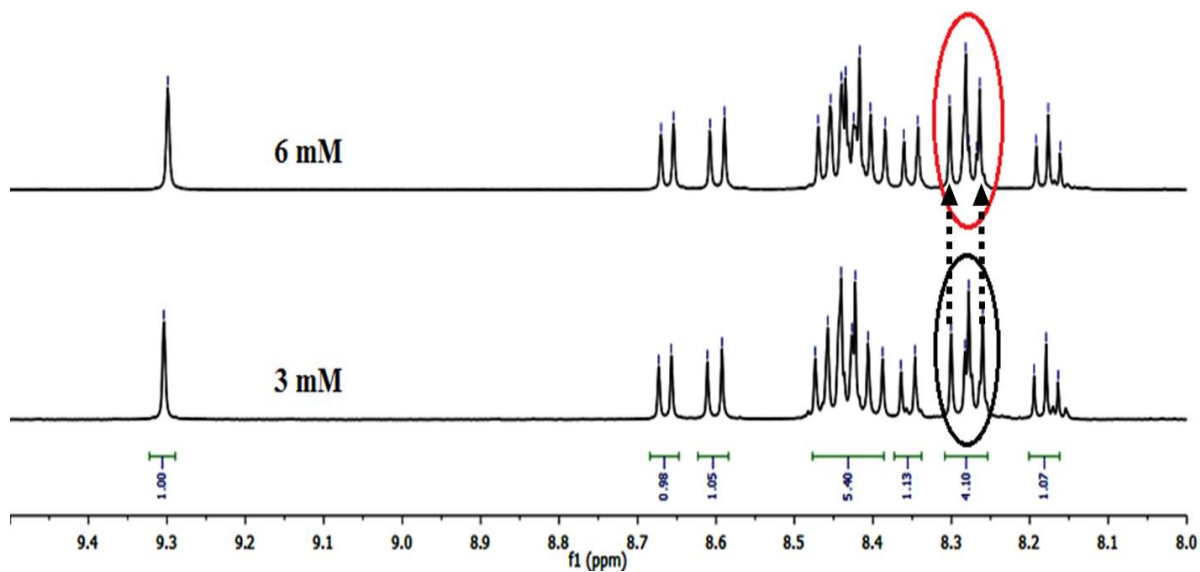
Fig. S11 Concentration dependent ^1H NMR profile of CN1 in DMSO-d_6 reveals downfield shifting of protons upon increasing concentration from 3 to 6 mM.
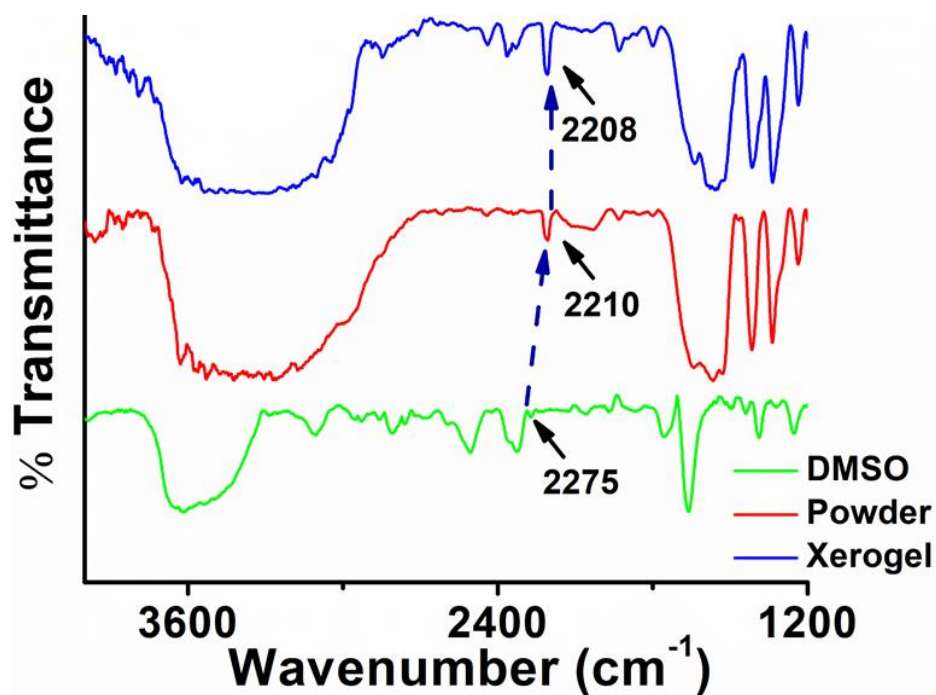
Fig. S12 FTIR spectra of CN1 reveal variation in cyanide stretching frequency on going from DMSO (10 μM), solid powder and gel (DMSO, 1 wt%).
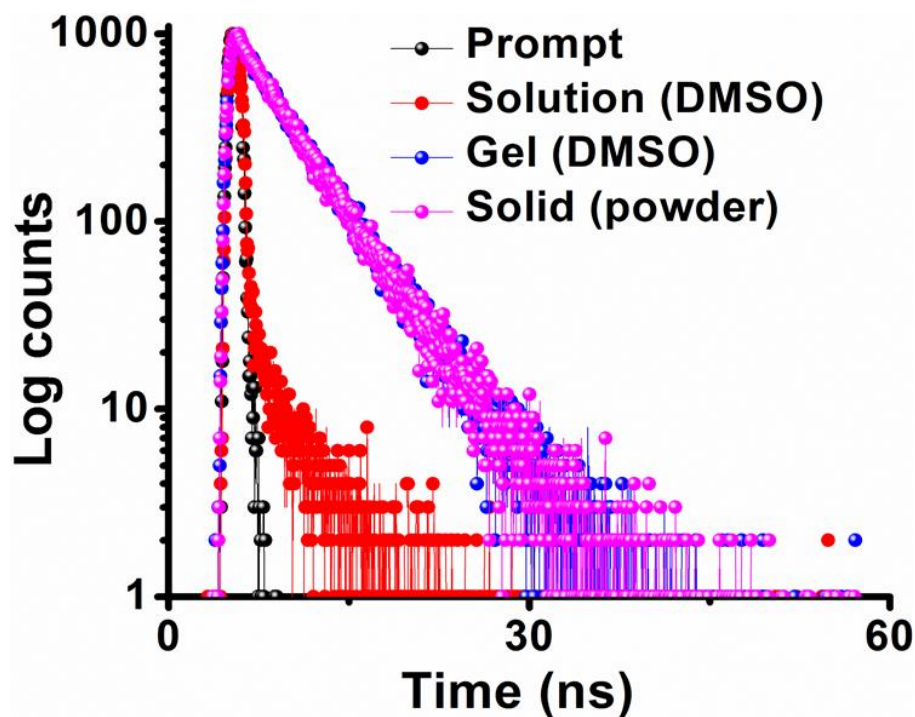
Fig. S13 Time resolved fluorescence decay profile of CN1 in solution (10 μM), gel (DMSO, 1 wt%) and solid (powder).
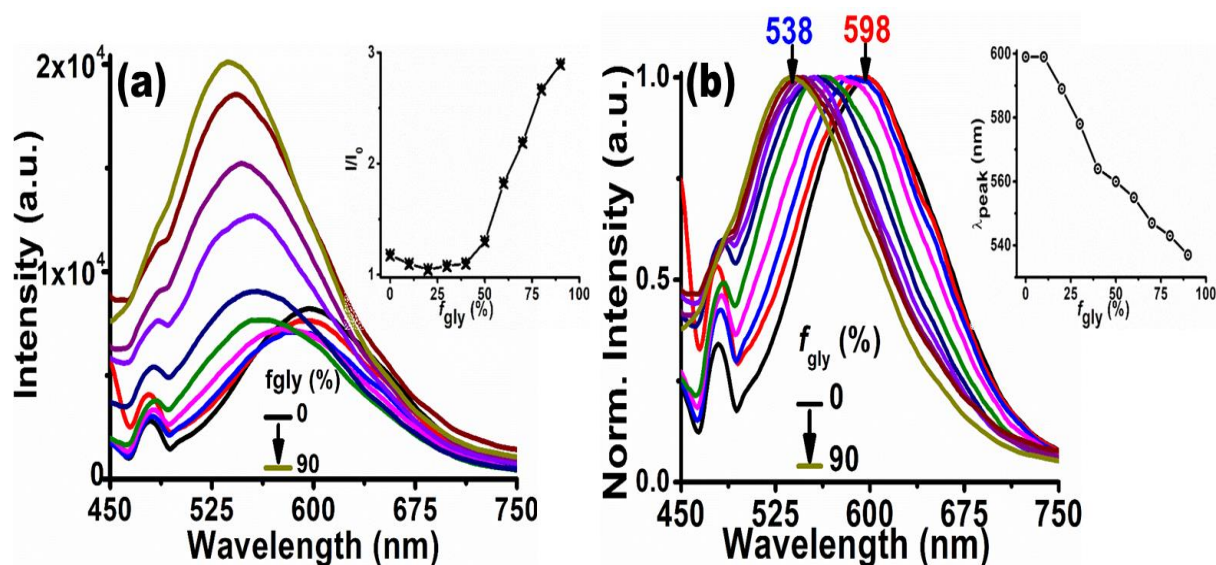
Fig. S14 (a) Variation in PL spectra and relative peak intensity (Inset) of CN1 in DMSO (concentration = 10 μM, λ_{ex} = 420 nm) with increased f_{gly}(%)s. (b) Normalized emission spectra and variation in emission peak position (λ_{peak}) of CN1 (inset) in DMSO with increased f_{gly}(%)s. (concentration = 10 μM, λ_{ex} = 420 nm).
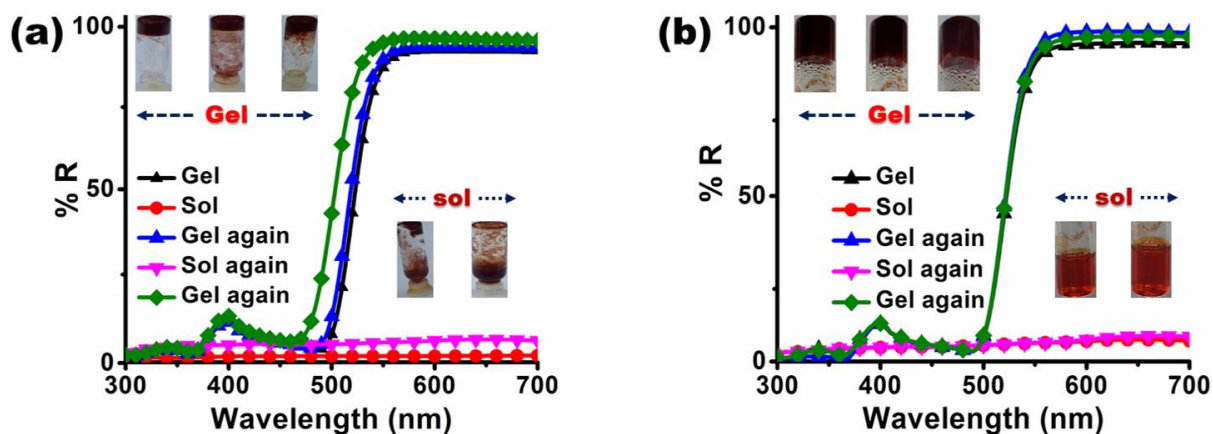
Fig. S15 Variations in diffuse reflectance UV/Vis absorption spectra of CN1 assembly during (a) shaking/resting and (b) heating/cooling events. Corresponding Insets denote photographs of CN1 assembly during (a) shaking/resting and (b) heating/cooling events.
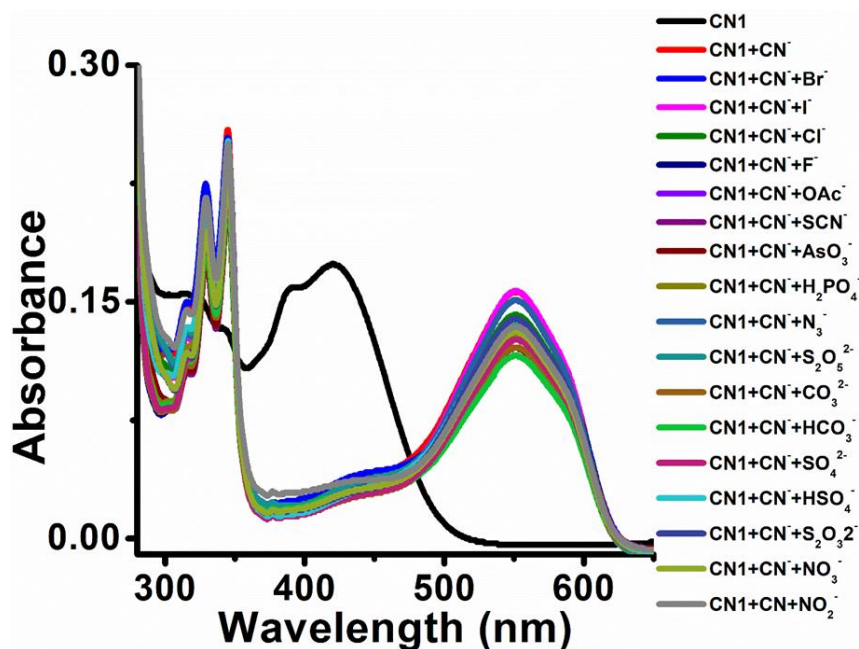
Fig. S16 Absorption spectra of CN1 (10 µM) upon simultaneous addition of aqueous CN^- and excess aqueous solutions of other anions into DMSO/water mixture [8:2(v/v)].
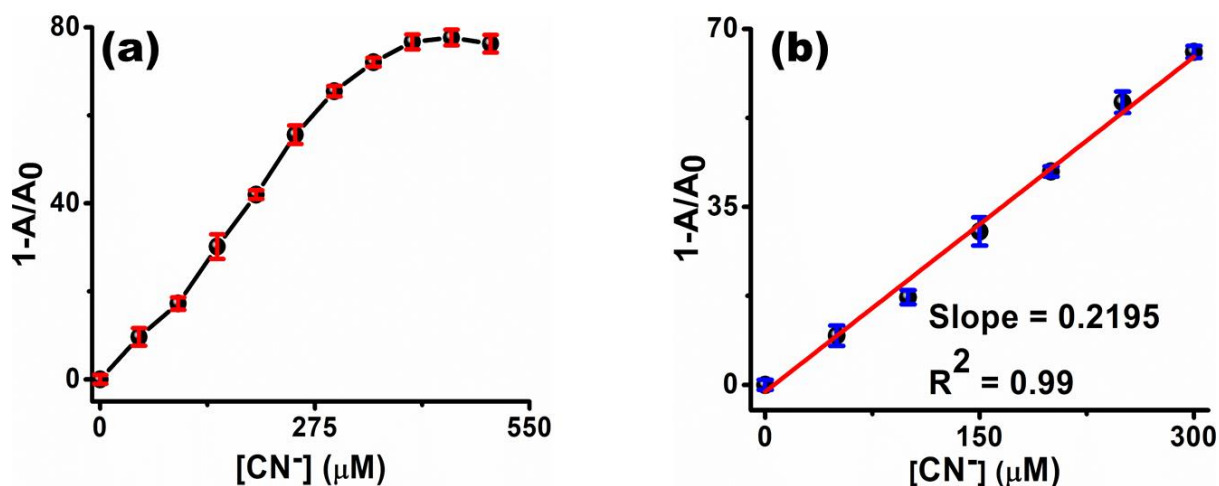
Fig. S17 (a) Variation in absorbance of CN1 in DMSO/water mixture [8:2(v/v)] with increased [CN⁻] (concentration = 10 µM). (b) Linear variation in absorbance of CN1 (10 µM) in DMSO/water mixture [8:2(v/v)] with increased [CN⁻] (≤ 300 µM).

Benesi-Hildebrand equation:

The Benesi-Hildebrand equation for calculating binding constant between analyte and probe is given by the following equation:

$$\frac{1}{A-A_0} = \frac{1}{k_a(A_{max}-A_0)[CN^-]} + \frac{1}{A_{max}-A_0}$$ (S1)

Where, A = experimentally observed absorbance; A_0: absorbance of free probe; A_{max}: Saturated absorbance of probe-analyte association.
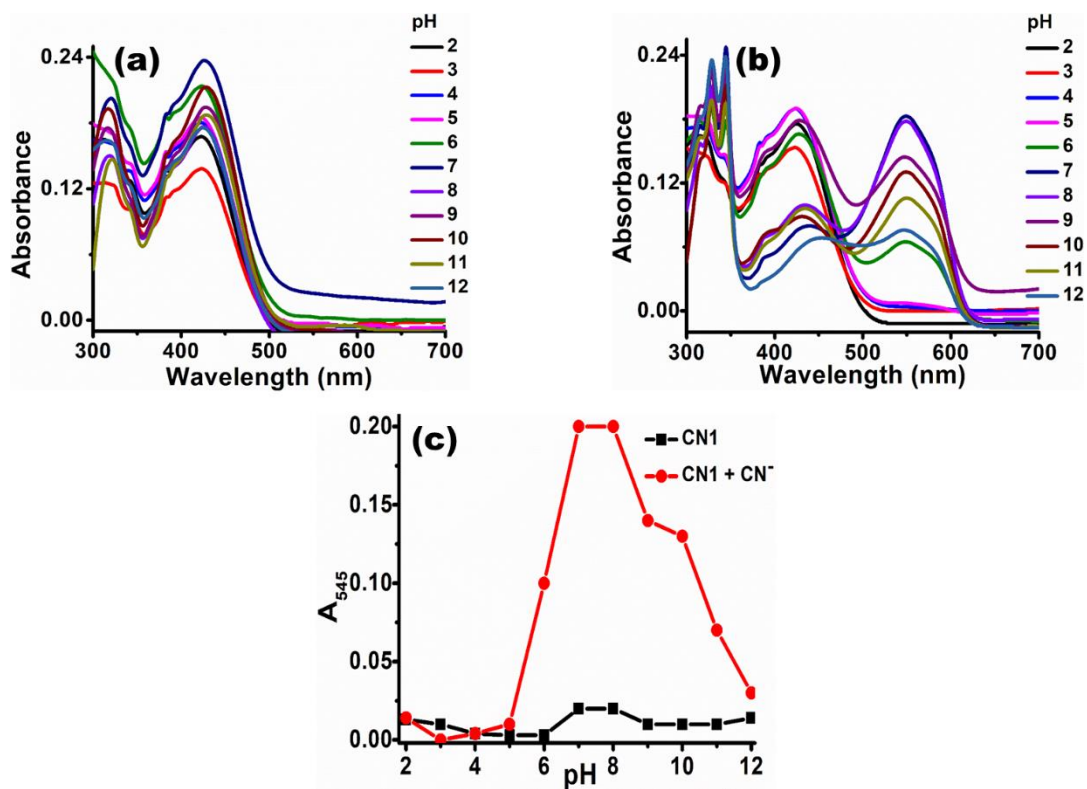
Fig. S18 Variations in UV/Vis absorption spectra of (a) CN1 and (b) CN1 after addition of CN^- (50 equiv.) with increased pH. (c) Change in absorbance at 545 nm of CN1 before and after addition of CN^- (50 equiv.) with increased pH condition.

Fig. S19 Photograph of CN1 coated glass slide taken under UV light ($\lambda_{ex} = 365$ nm).
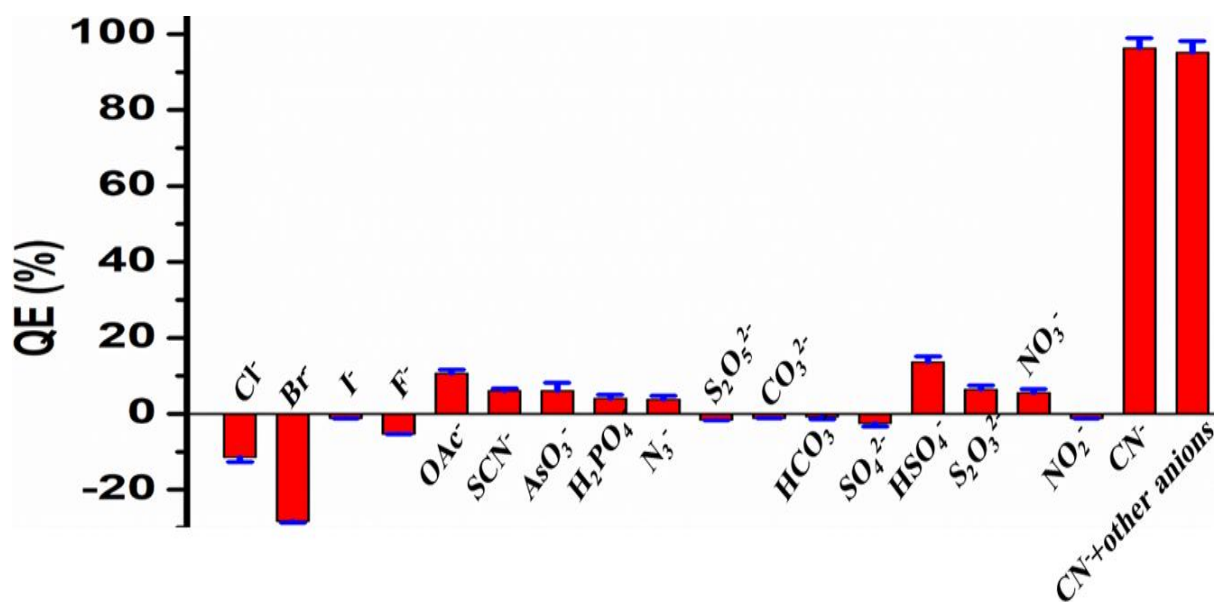
Fig. S20 Bar plot representing QE(%)s of CN1 as-synthesized powder towards different analytes and analyte mixture. The error bars for every measurement are included.
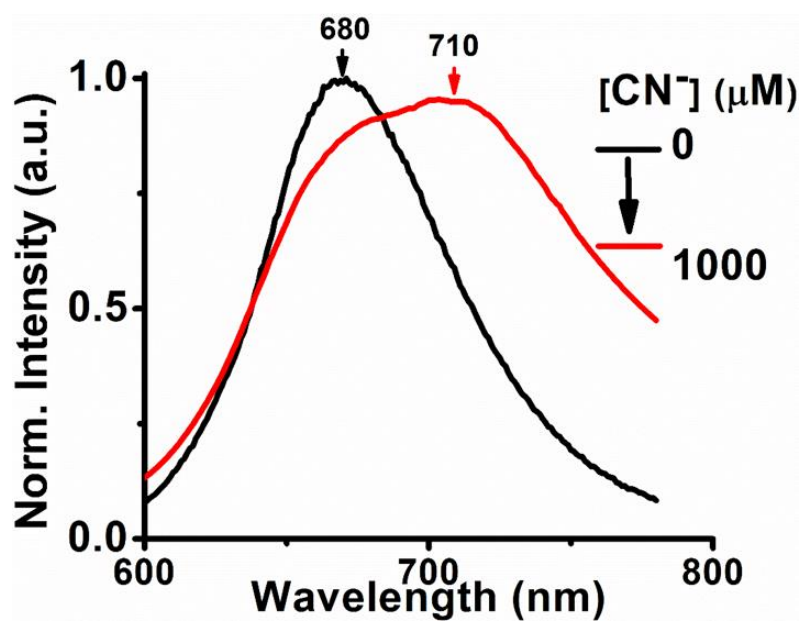
Fig. S21 Bathochromic shift in emission maxima of CN1 gel [8:2 (v/v)DMSO/water, 1 wt%] after treating aqueous solution of CN^- ($\lambda_{ex} = 450$ nm).
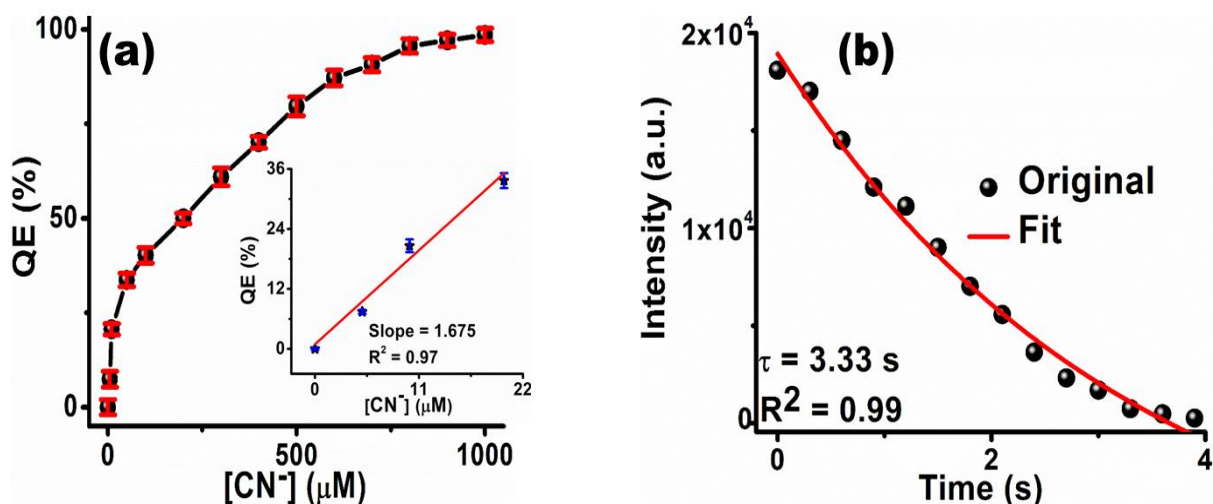
Fig. S22 (a) Variation in emission intensity of CN1 gel [8:2 (v/v) DMSO/water, 1 wt%] with respect to increased [CN⁻] (λ_{ex} = 450 nm). Inset represents linear variation in emission intensity with respect to lower [CN⁻]. (b) PL decay kinetics of CN1 gel [8:2 (v/v) DMSO/water, 1 wt%] at λ_f = 680 nm in presence of CN⁻.
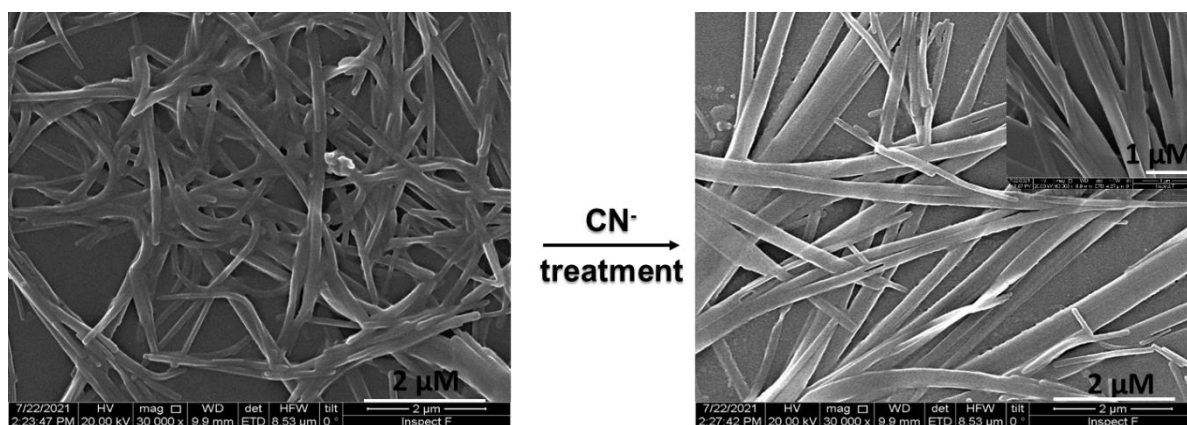
Fig. S23 SEM images of CN1 gel [8:2 (v/v) DMSO/water, 1 wt%] before (left) and after (right) treatment with aqueous solution of CN⁻. Corresponding inset represents retention of fibre tapes in cyanide treated gel.
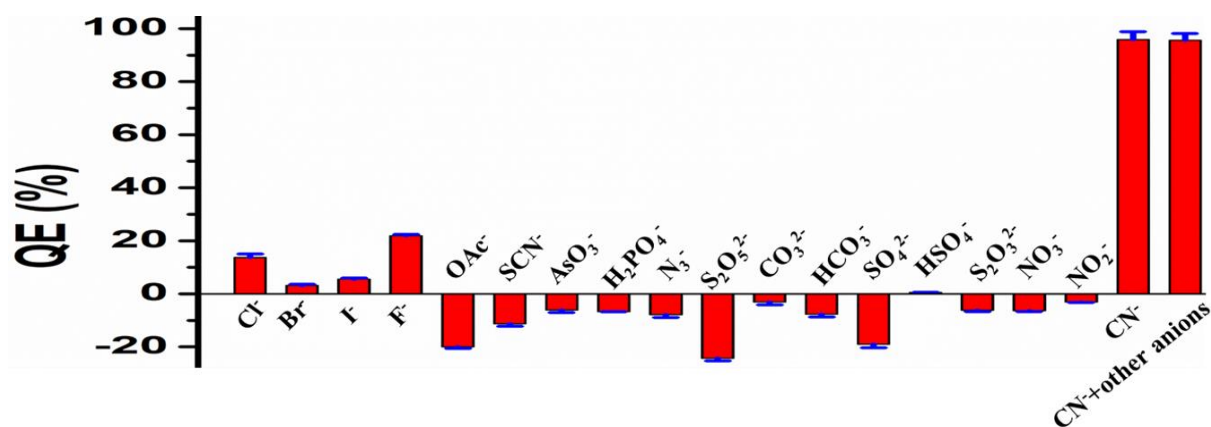
Fig. S24 Bar plot representing QE(%)s of CN1 gel [DMSO/water 8:2 (v/v), 1 wt%] towards different analytes and analyte mixture. The error bars for every measurement are included.

Stern-Volmer equation:

The nature of binding interaction between analyte and probe was determined based on Stern-Volmer equation.

$$\frac{I_0}{I} = 1 + K_{SV}[Q] \tag{S2}$$

where, I_0 and I are the fluorescence intensity of probe in absence and presence of analyte, K_{SV} is the Stern-Volmer constant, and $[Q]$ is the analyte concentration.
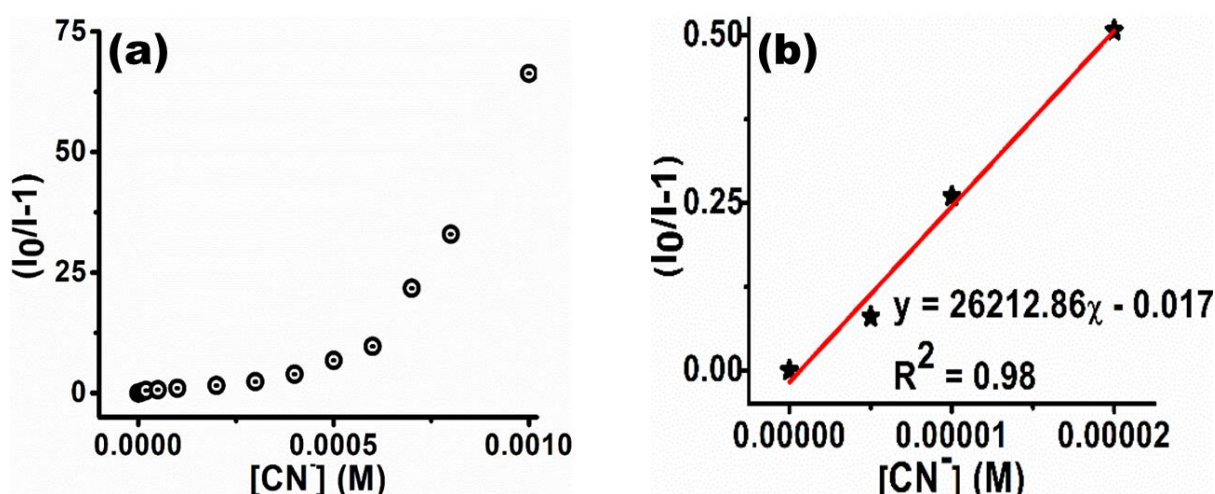
Fig. S25 (a) Variation in emission spectra of CN1 with increased [CN-] based on Stern-Volmer equation. (b) Linearly varied emission intensity of CN1 under lower [CN-] according to the Stern-Volmer equation.
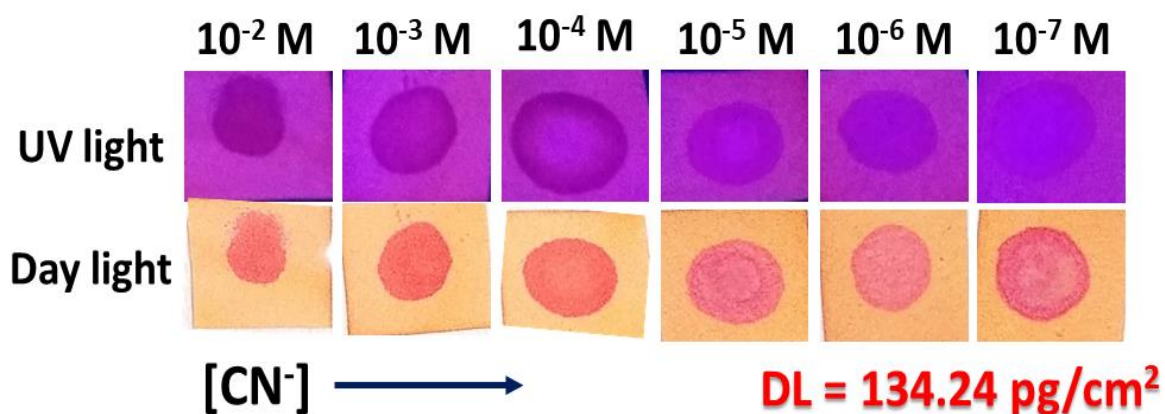
Fig. S26 Fluorogenic (upper panel) and colorimetric (down panel) dual channel contact mode detection of aqueous CN- based on CN1 xerogel film observed under both UV (λ_{ex} = 365 nm) and day light.

Calculation of DL based on dual channel contact mode detection of CN⁻

From Fig. S26, it can be observed that the fabricated strips were capable to detect CN⁻ from water until the limit of 1×10^{-7} M. Based on the above observation, detection limit (DL) of CN1 strips towards aqueous CN⁻ was calculated to be as low as 134.24 pg/cm², by pressing 5 μL of 1×10^{-7} M aqueous CN⁻ solution on the strip, covering 1cm² area using analyte strained brush.

The quantitative analysis of DL is as follows:

$DL = [10^{-7} \text{ mol/L} \times 268.48 \text{ g/mol} \times 5\times10^{-6} \text{ L}]/\text{cm}^2$

$= 134.24\times10^{-12} \text{ g/cm}^2$

$= 134.24 \text{ pg/cm}^2$; where molecular weight of tetrabutylammonium cyanide (acted as source of CN⁻) = 268.48 g/mol.

For getting accuracy the experiment was repeated where, minimum detected concentration of CN⁻ by the kits was obtained as similar as 1×10^{-7} M with DL of 134.24 pg/cm², by adding 5 μL of 1×10^{-7} M aqueous CN⁻ solution on the strip, covering 1cm² area.
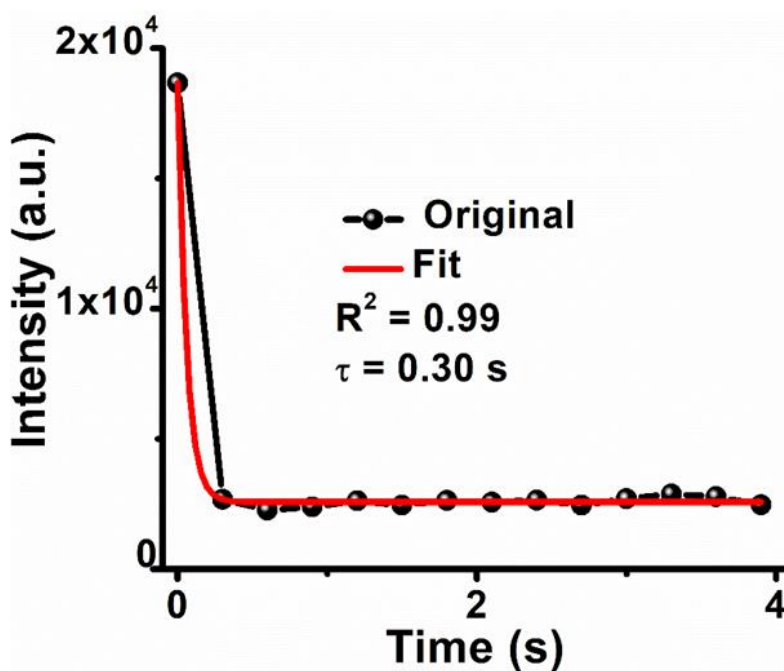
Fig. S27 Single exponentially fitted PL decay kinetics of as-synthesized CN1 film ($\lambda_f = 680$ nm).
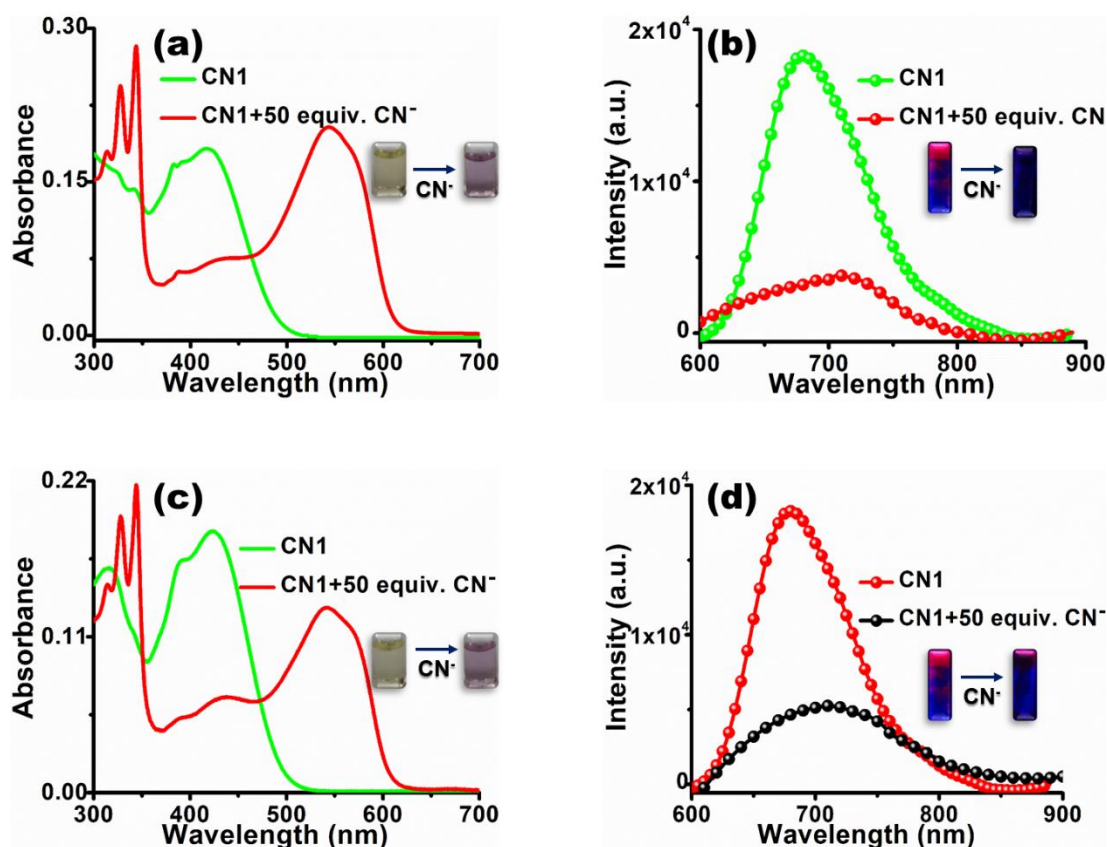
Fig. S28 Variations in (a, c) UV/Vis absorption and (b, d) emission spectra of CN1 solution (concentration = 10 μM) and gel (1 wt%) respectively in (a, b) 8:2 (v/v) DMSO/HEPES and (c, d) 8:2 (v/v) DMF/HEPES solvent mixtures in presence of CN⁻ (50 equiv.). Corresponding insets denote UV-photographs of dual channel colorimetric (a, c) and fluorogenic (b, d) sensory responses of CN1 both in solutions and gel states.
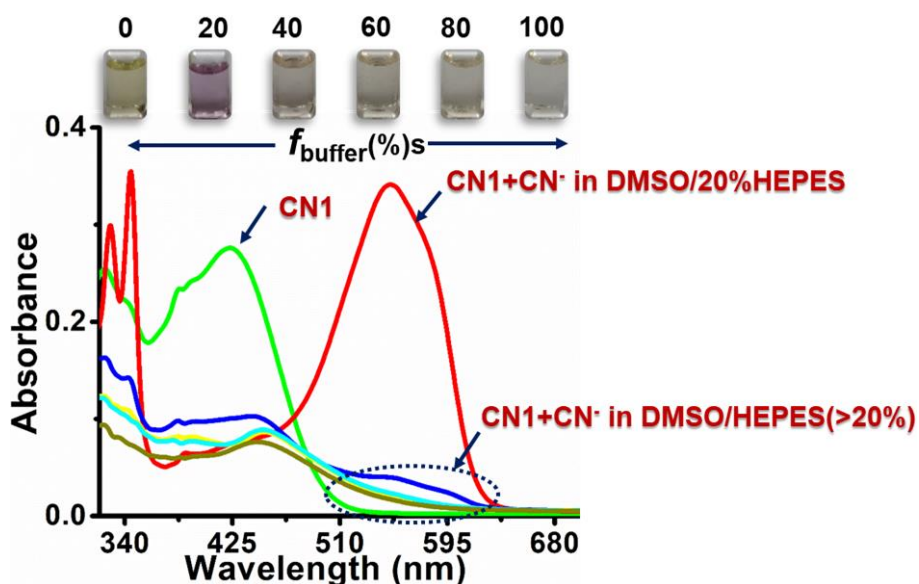
Fig. S29 UV/Vis absorption spectral responses of CN1 (concentration = 10 μM) in DMSO with increased f_{buffer}(%)s in presence of CN⁻ (50 equiv.). Corresponding upper panel of the figure represents naked eye variations in solution colors of CN1 in DMSO with increased f_{buffer}(%)s in presence of CN⁻ (50 equiv.).

S23

Table S5 Comparison table of CN1 with previously reported CN⁻ sensors.

Reference	Properties studied	Sensory response			Practical applications	Sensing events in environmental water samples	Sensing events in food samples	quantitative detection of CN⁻ in food samples	Other practical applications
		solution	solid	gel					
[10]	CN⁻ sensing via displacement strategy	5.77 µM/6.42 µM	-	-	YES	-	-	-	Cyanide sensing in mouse serum and cell imaging
[11]	Ratiometric cyanide sensing	11 nM	Paper strips (~2.6 ng/cm²)	-	YES	YES	-	-	-
[12]	Colorimetric and ratiometric cyanide sensing	5.77×10^{-8}M	-	-	-	-	-	-	-
[13]	Reaction based colorimetric cyanide sensing	1.1 µM	-	-	YES	YES	-	-	-
[14]	Dual-channel (Fluorescent and colorimetric) cyanide sensing	800 nM	-	-	YES	-	-	-	-
[15]	Dual-channel cyanide sensing	4.27×10^{-7}M	Paper strips (8×10^{-3} M)	-	YES	YES	-	-	-
[16]	Optical sensing of cyanide based on nucleophilic reaction	24.5, 1.70 and 5.07 µM	Paper strips (0.5 mM for all three probes)	-	YES	-	-	-	-
[17]	Colorimetric cyanide sensing	7.08 µM	Paper strips	-	-	-	-	-	-
[18]	Colorimetric and fluorogenic cyanide sensing	0.32 µM (8 ppb) and 0.57 µM (14 ppb)	-	-	-	-	-	-	-
[19]	visual sensing of cyanide	9.36×10^{-6}M	-	Gel-to-sol	-	-	-	-	Reversible thermochromism in gel
[20]	Dual-channel cyanide sensing	2.8×10^{-7}mol/L	Paper strip	-	-	-	-	-	-
[21]	Colorimetric	2.8×10^{-7}	-	-	-	-	-	-	-

Ref	Type	LOD	Col4	Col5	Col6	Col7	Col8	Col9	Col10
	and fluorogenic cyanide sensing	mol/L							
[22]	Colorimetric and fluorogenic cyanide sensing	4.97×10^{-7} M	Paper strip	-	-	-	-	-	-
[9]	Colorimetric and fluorogenic cyanide sensing	39.9 nM	Paper strip	-	YES	YES	YES	-	-
[23]	Colorimetric and fluorogenic cyanide sensing	3.8×10^{-8} M	-	-	-	-	-	-	Detection of trace amount of water in organic solvents (THF, 1,4-dioxane)
[24]	Colorimetric and fluorogenic cyanide sensing	qualitative detection	Paper strip (18 µM)	-	YES	-	-	-	Sensing of organic solvents and water in organic mediums
[8]	Colorimetric and fluorogenic cyanide sensing	5.81×10^{-8} M	Paper strip	-	YES	-	YES	In average 5.92 µM§ (from sprouted potato)	-
[25]	Dual channel cyanide sensing	Qualitative visual detection	Paper strip		YES	YES (visual detection)	-	-	-
[26]	Colorimetric and fluorogenic cyanide sensing	1.73×10^{-8} M, 4.36×10^{-8} M	Qualitative fluorescence and color imaging on paper strip	-	-	-	-	-	-
[27]	Chemodosimetric cyanide sensing	4.26 µM	Probe coated silica plate	-	-	-	-	-	-
[28]	Colorimetric and fluorogenic cyanide sensing	39.3 nM	Test paper kits	-	YES	YES	-	-	-
[29]	Naked eye detection of cyanide	1.5 µM	-	Gel-to-sol	YES	-	YES	-	-
[30]	Cyanide sensing via displacement strategy	-	Test strip	1.09 µM	-	-	-	-	-
[31]	Colorimetric cyanide	1.36×10^{-4} mol/L	-	Gel-to-gel	-	-	-	-	Gel-to-gel and Gel-to-sol

Ref	Method	LOD	Form	Gel					Application
	sensing								induced sensing of Hg (II) and Cu(II)
[32]	Dual-channel cyanide sensing	0.5 µM	Solid powder	-	YES	-	YES	-	-
[33]	Fluorescent and colorimetric cyanide sensing	3.02×10^{-6} M	-	Gel-to-gel	YES	-	-	-	Detection of Al^{3+}, Fe^{3+} and L-Cys via multi-analyte sensing arrey
[34]	Fluorescence quenching assisted cyanide sensing via mettalogel	-	-	Gel-to-gel (4.8×10^{-5} M)	-	-	-	-	Dynamic Sensing of Br^{-} SCN^{-}, S^{2-}
[35]	Colorimetric and fluorogenic sensing of cyanide	0.46 µM	Test strips	-	YES	-	YES	-	Cell imaging
Present study	Colorimetric and fluorogenic cyanide sensing	5.42±0.256 nM (chromogenic)	Paper strips (134.24 pg/cm^2)	Gel-to-gel (0.48±0.01 µM) (fluorogenic)	YES	YES (qualitative and quantitative detection)	YES (qualitative and quantitative detection)	Sprouted potato (5.89±0.201 µM); Apple seeds (6.18±0.043 µM); Bitter seeds (6.06±0.106 µM); Sudan grasses (5.19±0.15 µM)	Thixotropic and thermochromic 'ON-OFF' GIEE switching and superhydrophobic surface formation

§Calculated by averaging the detected CN$^-$ concentrations.
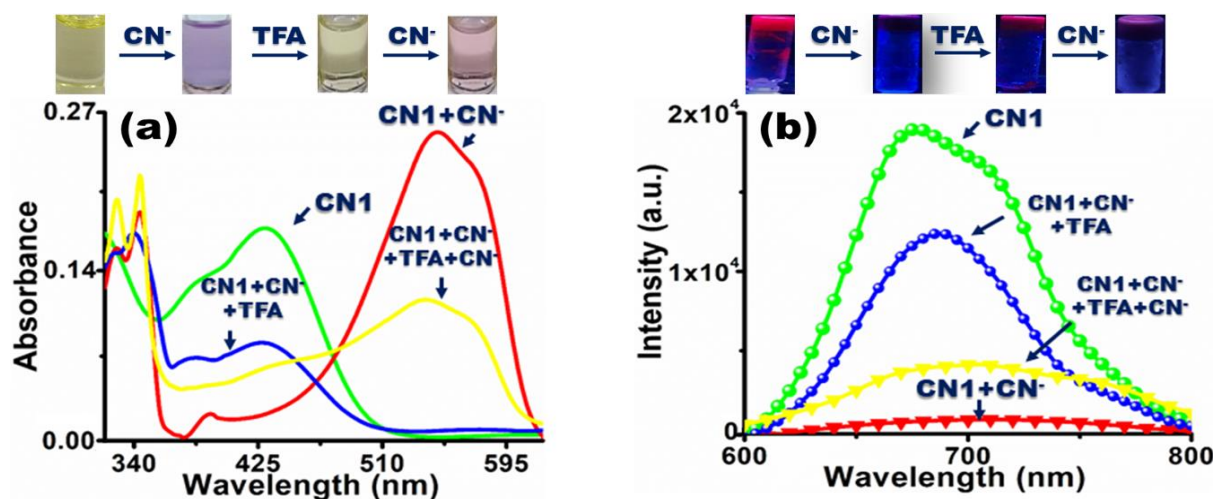
Fig. S30 (a) Variations in UV/Vis absorption and (b) emission spectral responses (λ_{ex} = 450 nm) of CN1 in 8:2 (v/v) DMSO/water (concentration = 10 μM) and gel [1 wt%, 8:2 (v/v) DMSO/water] respectively upon simultaneous addition of CN⁻ (50 equiv.) and TFA (100 equiv.). Upper panel of figures indicate photographs of CN1 during simultaneous addition of CN⁻ and TFA observed under day and UV light.
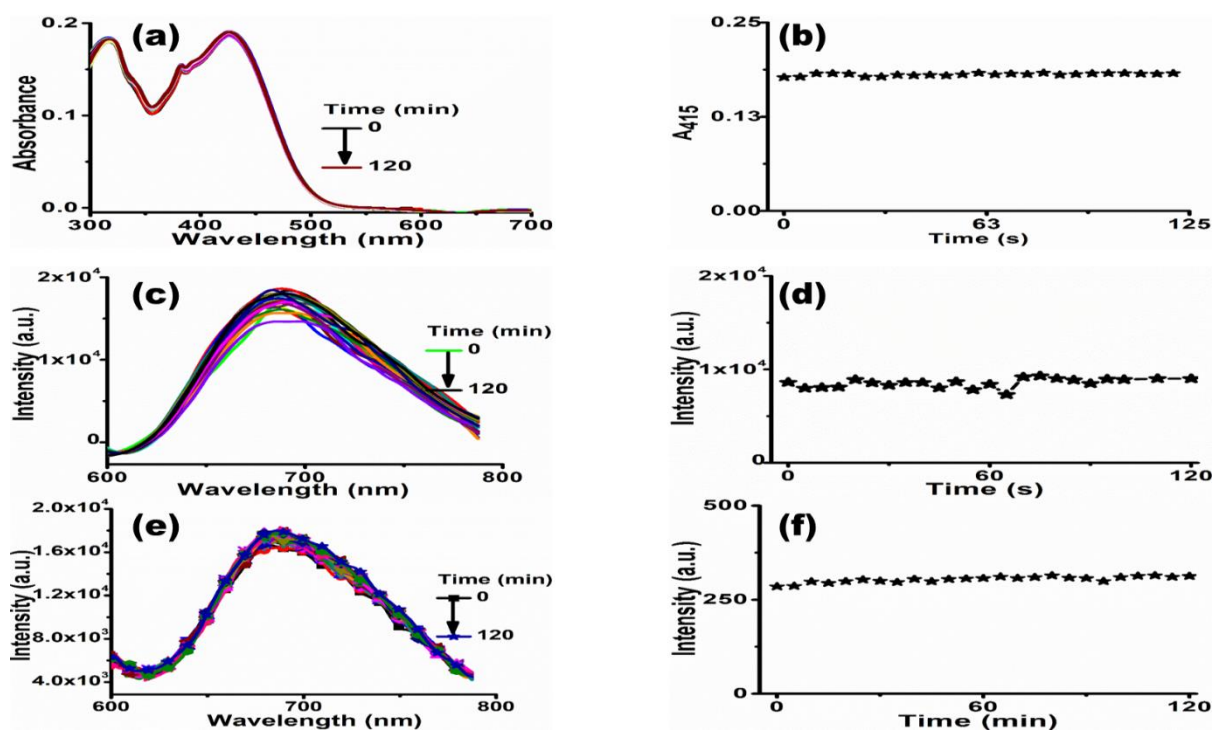
Fig. S31 (a) Variation in UV/Vis absorption and (b) time-dependent change in absorbance at λ = 415 nm of CN1 (concentration = 10 μM) in 8:2 (v/v) DMSO/water after UV-irradiation for 120 minutes. (c, e) emission spectra (λ_{ex} = 450 nm) and (d, f) time-dependent change in emission intensity of CN1 in (c, d) 8:2 (v/v) DMSO/water gel (1 wt%) and (e, f) as-synthesized thin film after UV irradiation for 120 minutes.
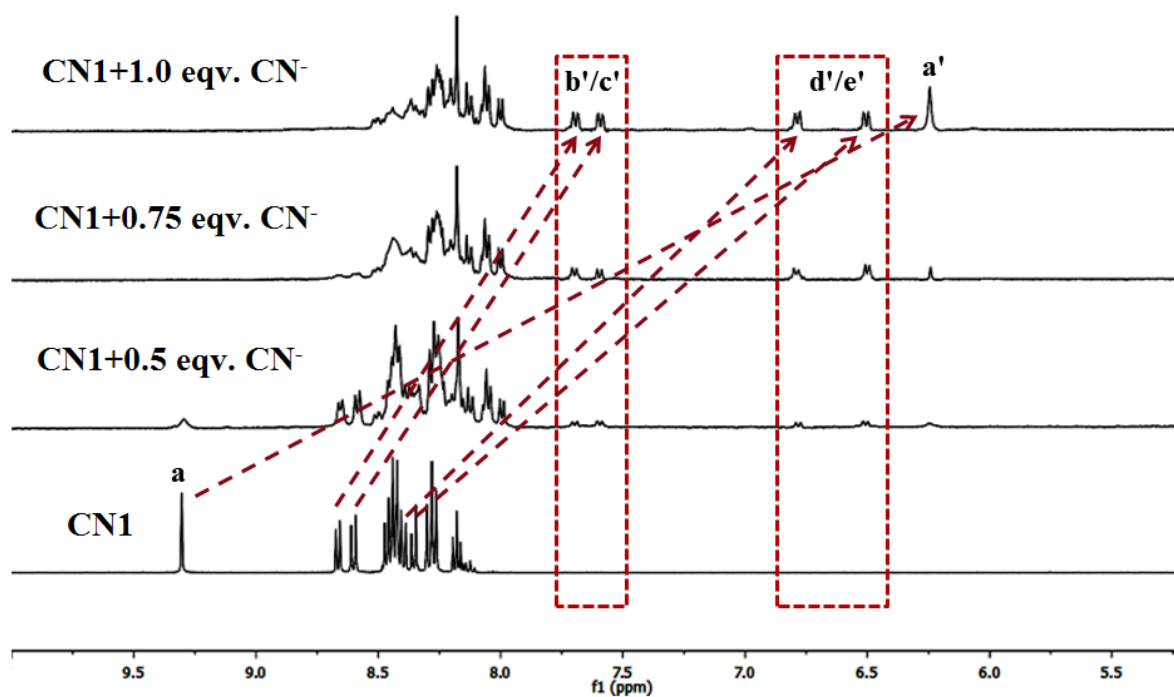
Fig. S32 ^{1}H NMR spectral response of CN1 in DMSO-d_6 in presence of increased [CN$^-$].

Table S6 Analysis of ^{1}H NMR titration of CN1 in presence of increased [CN$^-$].

CN1		[CN1-CN$^-$]	
Protons	δ (ppm)	Protons	δ (ppm)
H$_a$	9.304	Pyrene H$_s$	8.018-8.448
H$_b$/H$_c$	8.673,8.657/8.611,8.592	H$_{b'}$/H$_{c'}$	7.717,7.689/7.612,7.583
H$_g$ & H$_e$	8.388-8.473	H$_{d'}$/H$_{e'}$	6.836,6.802/6.520,6.488
H$_d$	8.364,8.346	H$_{a'}$	6.294
H$_h$	8.257-8.297		
H$_f$	8.194,8.179,8.164		
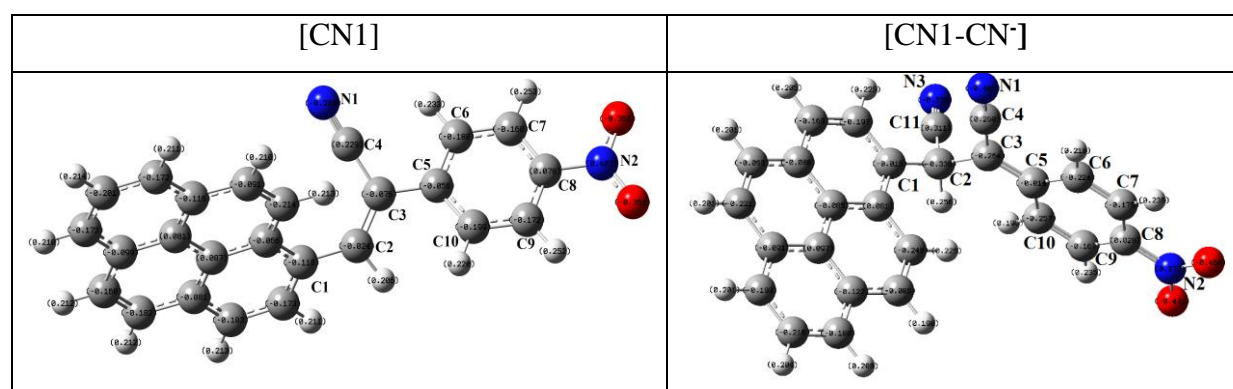
Fig. S33 The optimized geometry structures of [CN1] and [CN1-CN$^-$] with some selected atomic labelling with charge distribution (in b3lyp method and 6311(+)g basis set).

Table S7 NBO atomic natural charges calculated at b3lyp method with 6311(+)g basis set.

Atom	[CN1]	[CN1-CN⁻]
C1	-0.118	-0.015
C2	-0.024	-0.388
C3	-0.076	-0.264
C4	0.229	0.260
C5	-0.056	-0.014
C6	-0.188	-0.224
C7	-0.168	-0.175
C8	0.078	0.028
C9	-0.172	-0.167
C10	-0.199	-0.257
N1	-0.289	-0.406
N2 (NO$_2$)	0.407	0.373
N3 (CN)	---	-0.355
C11 (CN)	---	0.311
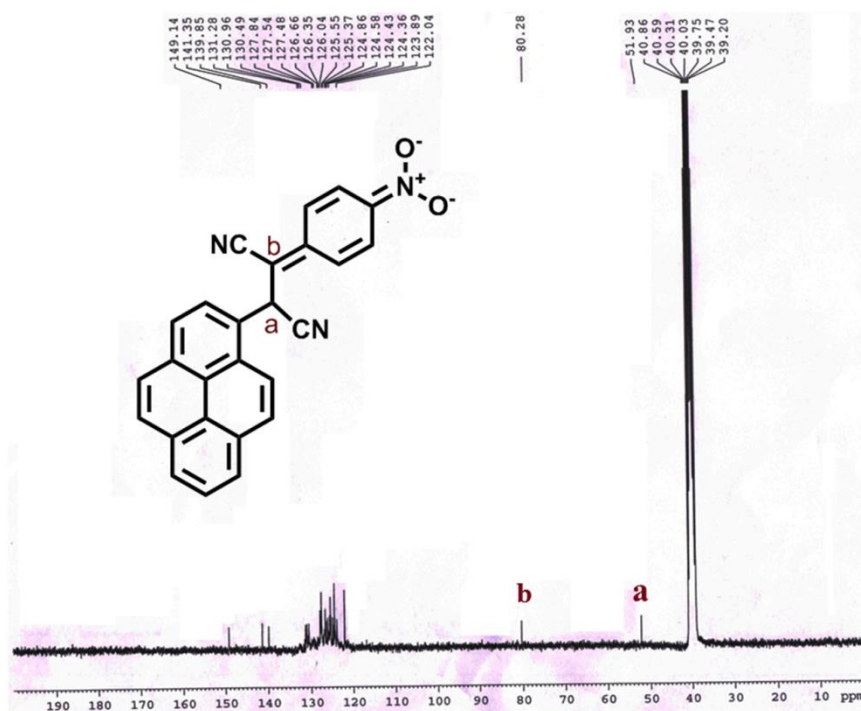
Fig. S34 ^{13}C NMR spectrum of [CN1-CN⁻] adduct in DMSO-d$_6$.

^{13}C NMR (125 MHz, DMSO-D$_6$): δ 149.14, 141.35, 139.85, 131.28, 130.96, 130.49, 127.84, 127.54 (2C), 127.48, 126.66, 126.35, 126.04, 125.55, 125.37 (2C), 124.86, 124.58, 124.43, 124.36 (2C), 123.89, 122.04 (2C), 80.28, 51.93.
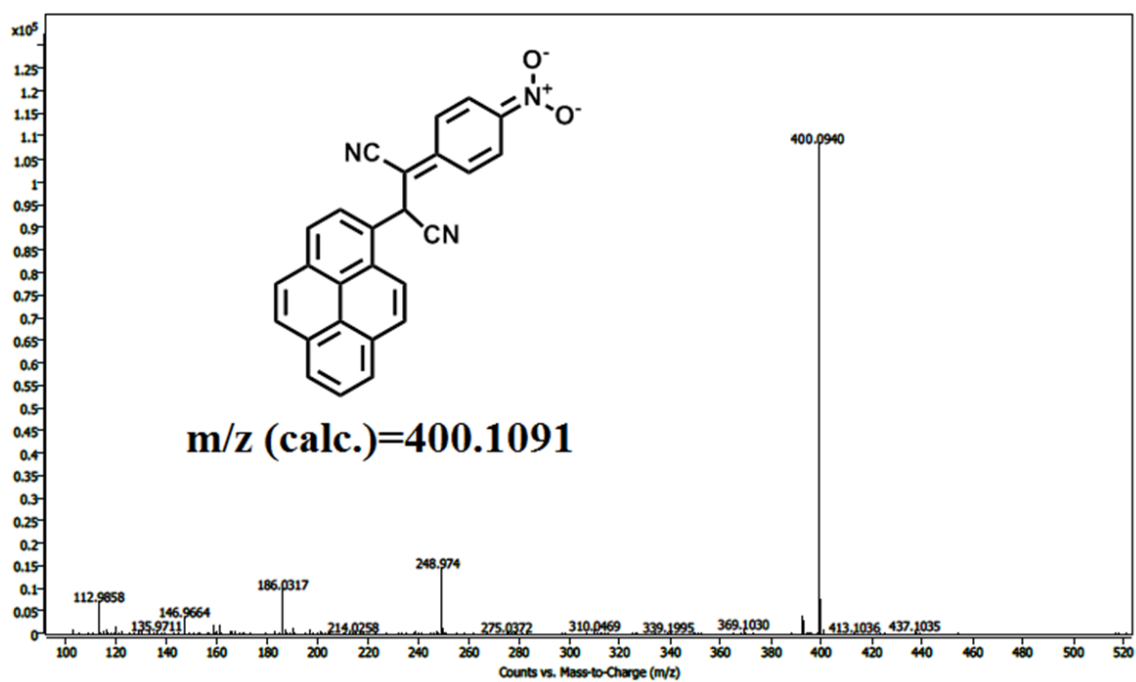
Fig. S35 HRMS plot [CN1-CN⁻] adduct.
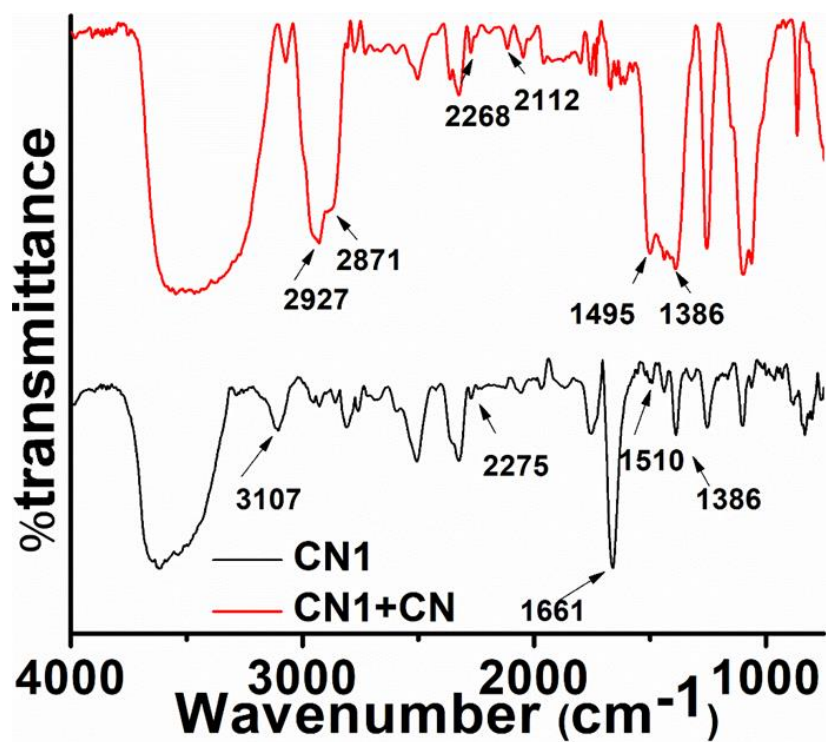
Fig. S36 FTIR spectra of CN1 and [CN1-CN⁻] adduct.
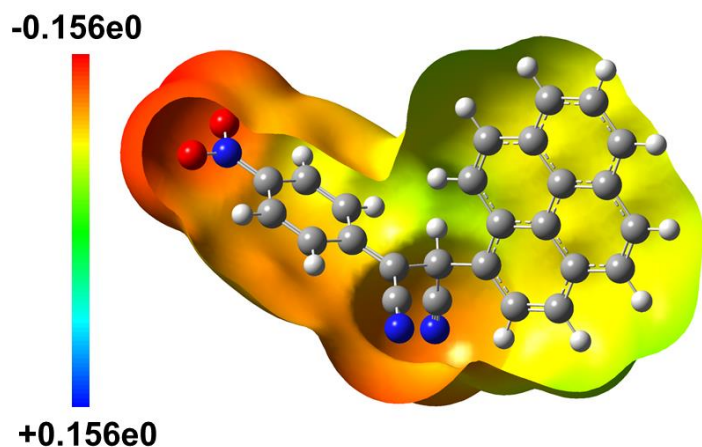
Fig. S37 Electrostatic potential map of [CN1-CN⁻] adduct based on b3lyp/6311(+)g level of theory. Scale values are in kcal/mol.
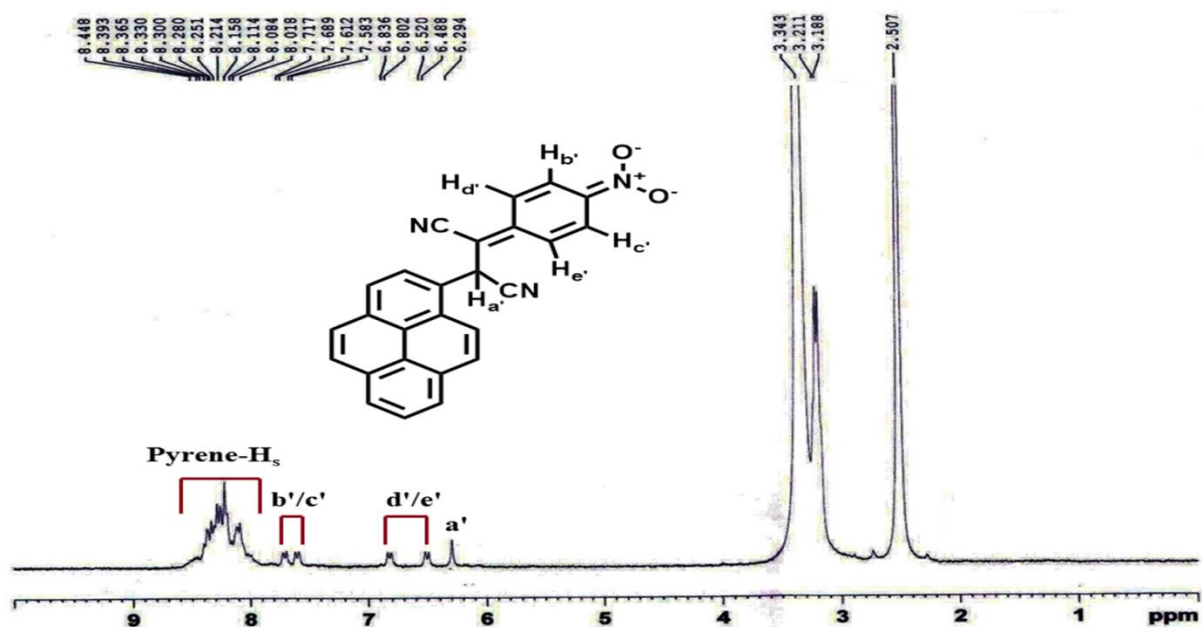
Fig. S38 ^{1}H NMR spectrum of [CN1-CN⁻] adduct.
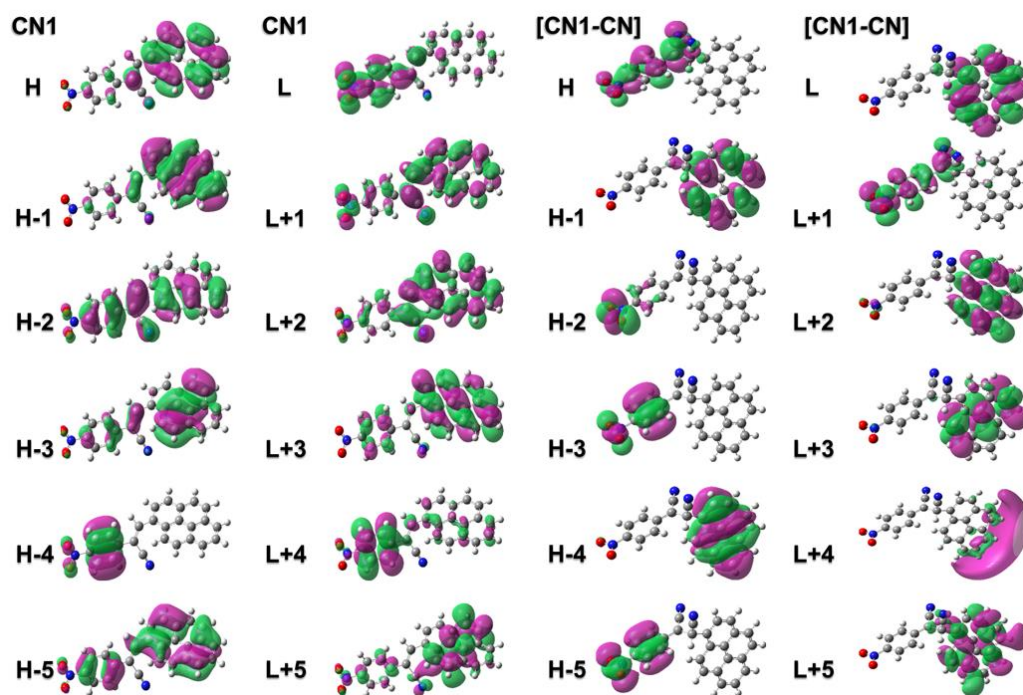
Fig. S39 Participating MOs of CN1 and [CN1-CN⁻] adduct.

Table S8 Calculated optical transitions of CN1 and [CN1-CN⁻] adduct

Compound	Simulated vertical excitation energy (eV)	Experimentally observed transition energy (eV)	Major transition	Oscillator strength (f)
CN1	3.20	3.00	H-L (87%)	0.76
	3.76	3.18	H-1-L, (44%), H-1-L+1 (16%), H-L+2 (16%), H-L+3 (18%)	0.04
	4.25	3.65	H-L+1 (59%), H-L+2 (15%)	0.16
	4.47	3.90	H-2-L (53%), H-1-L (10%)	0.3
[CN1-CN⁻]	2.45	2.26	H-L (96%)	0.10
	3.30	3.60	H-L+1 (29%), H-L+2 (66%)	0.85
	3.93	3.76	H-1-L	0.26
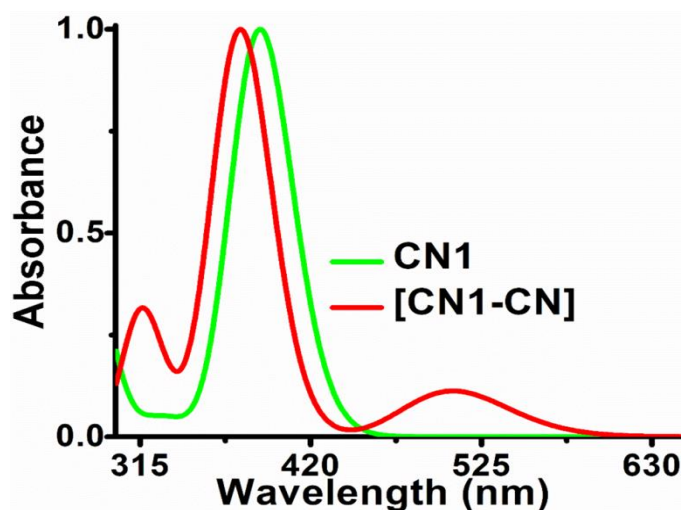
Fig. S40 Simulated UV/Vis absorption spectra of CN1 and [CN1-CN$^-$] adduct obtained from td-cam-b3lyp/cc-pVDZ level of theory.
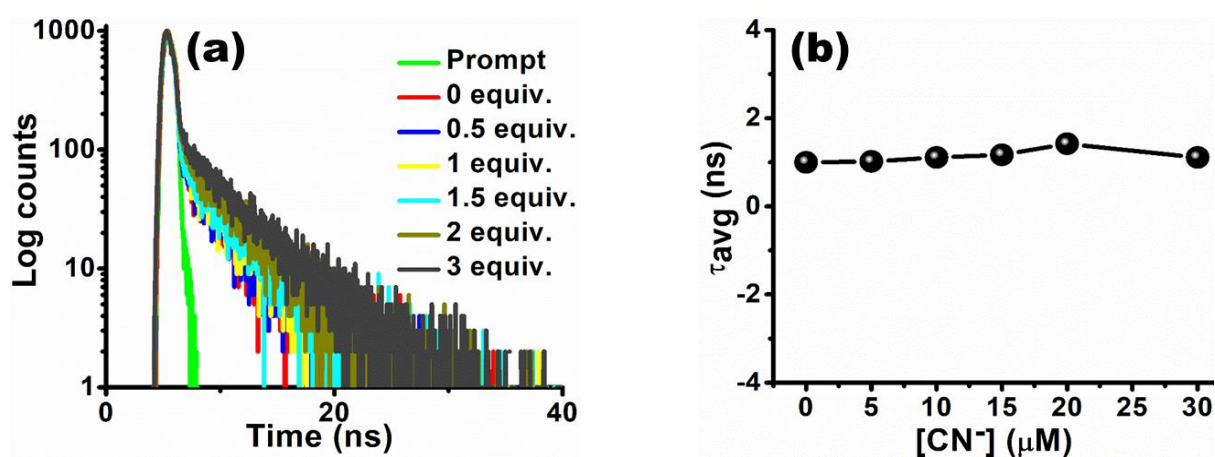
Fig. S41 (a) Time resolved fluorescence decay profile of CN1 in DMSO/water [8:2 (v/v)] upon increased [CN$^-$]. (b) Plot of τ_{avg} (ns) with respect to increased [CN$^-$].

Table S9 Time resolved fluorescence decay parameters of CN1 with increased [CN$^-$]

[CN1-CN$^-$] (μM)	τ_{avg} (ns)
0	0.96
5	1.02
10	1.11
15	1.17
20	1.42
30	1.11

Synthesis and characterization of F1

 [2-(4-fluorophenyl)-3-(pyren-1-yl)acrylonitrile] (F1) was synthesized based on knoevenagel

condensation reaction between 4-fluorophenylacetonitrile and pyrene carboxaldehyde as

mentioned in scheme S2.[1,2] To an ethanolic solution of 4-fluorophenylacetonitrile (~ 2.2 mmol) were added pyrene-1-carboxaldehyde (500 mg, 2.17 mmol) and piperidine (~ 4.4 mmol) under hot condition and the reaction mixture was allowed to reflux for twenty four hours. Afterwards the resultant solution was cooled down and stirred for another 4/5 hours to obtain yellow solid. The precipitate was then washed carefully with hot methanol and dried under high vacuum. Finally, the crude product was subjected to recrystallization with THF/MeOH to afford yellow powder F1 (700 mg, 93%).
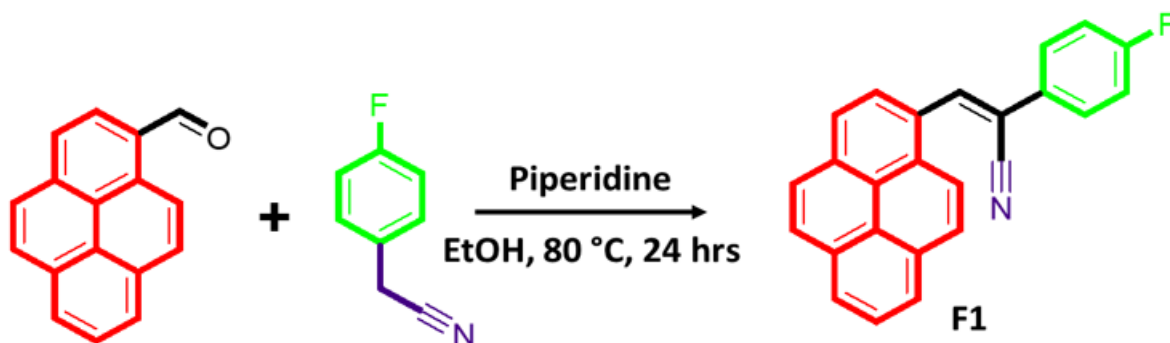
Scheme S2 Synthetic pathway for F1.
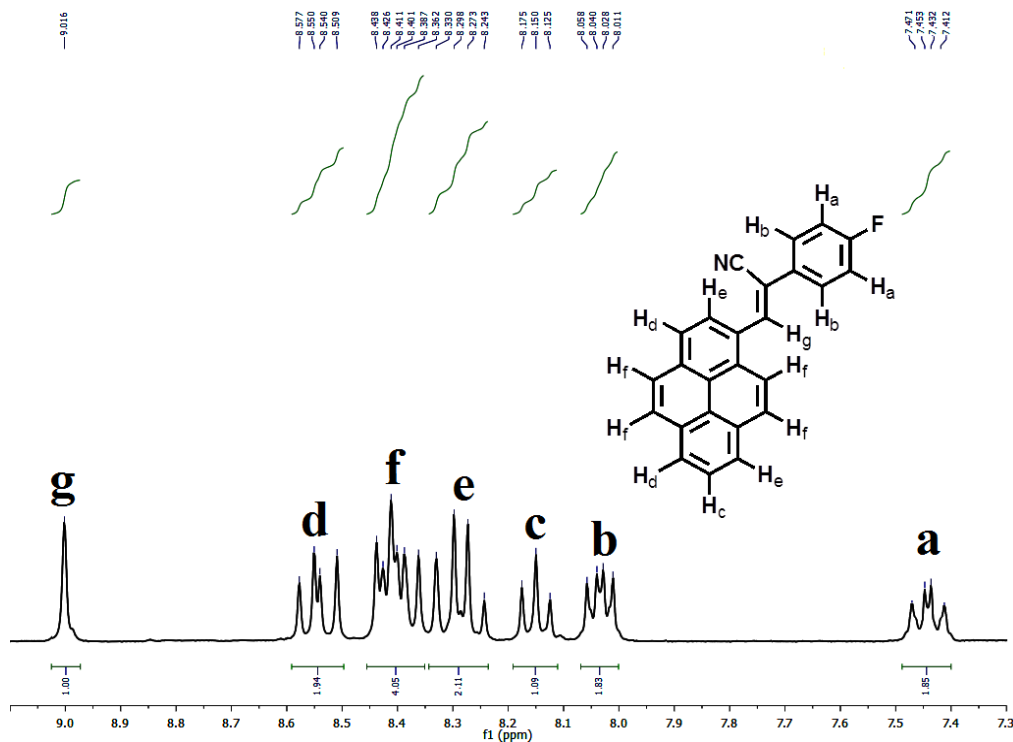
Fig. S42 ^{1}H NMR spectrum of F1 in DMSO-d[6].

M+H⁺ (Calculated) = 348.1189
Found = 348.1209
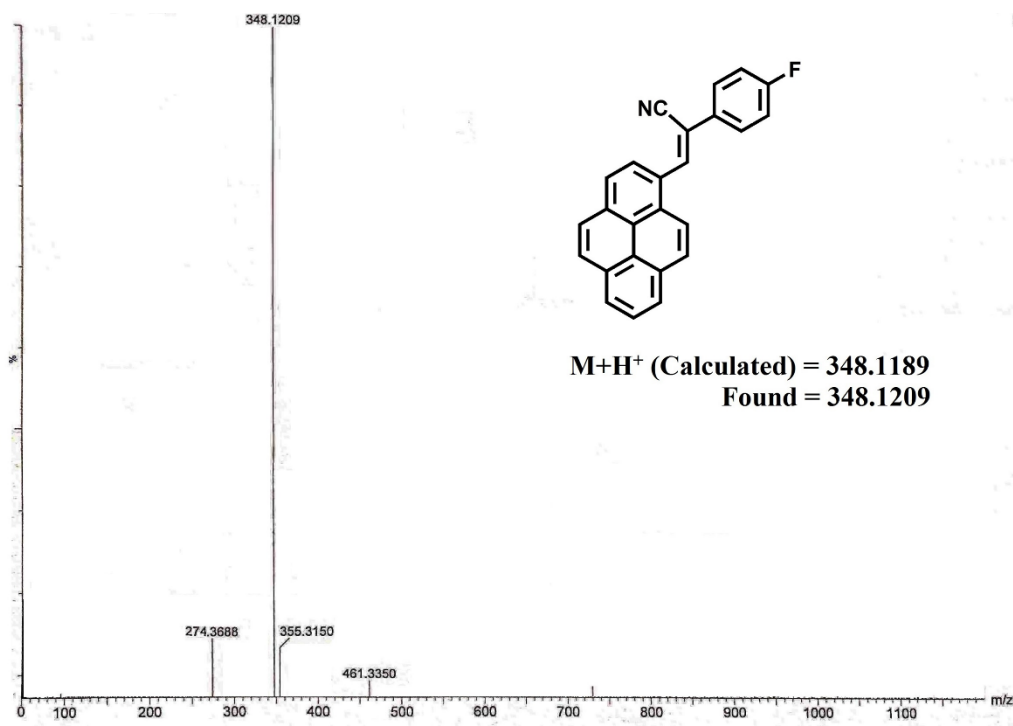
Fig. S43 ESI-MS spectrum of F1.
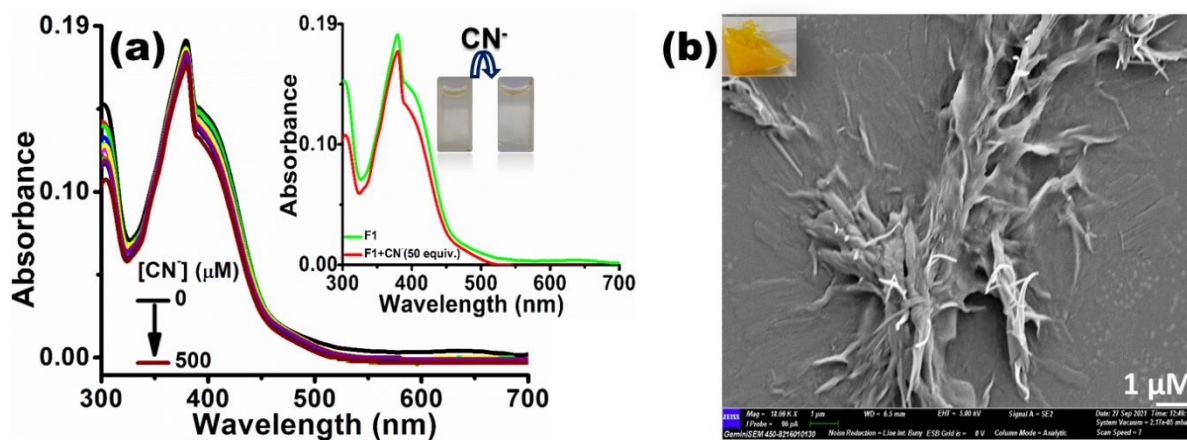
Fig. S44 (a) Variation in UV/Vis absorption spectra of F1 (10 µM) in presence of successively increased addition of CN⁻ concentration ([CN⁻], 0 - 50 equiv.). Corresponding inset represents UV/Vis absorption spectra of F1 (10 µM) before and after addition of 50 equiv. CN⁻ with respective photographs of solution colors taken under normal light. SEM image of extracted solid after heating/cooling treatment of F1 (1 wt%) in 8:2 (v/v) DMSO/water mixture. The image reveals existence of discontinued knotted bundles of aggregates. Corresponding inset represents the photograph of F1, taken under normal light after heating/cooling treatment.
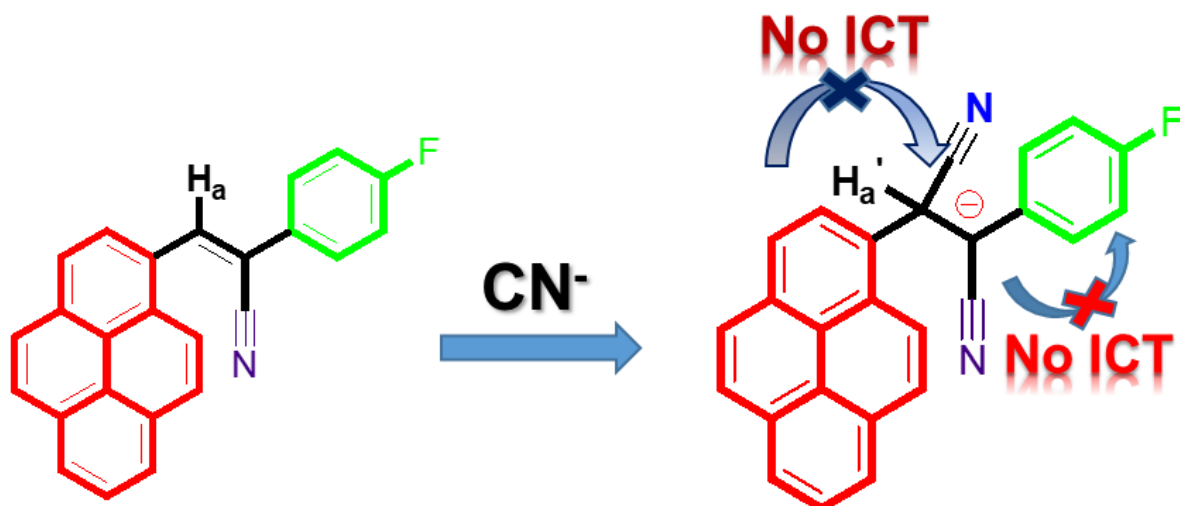
Scheme S3 Possible mechanistic pathway behind the spectral response of F1 towards CN⁻.
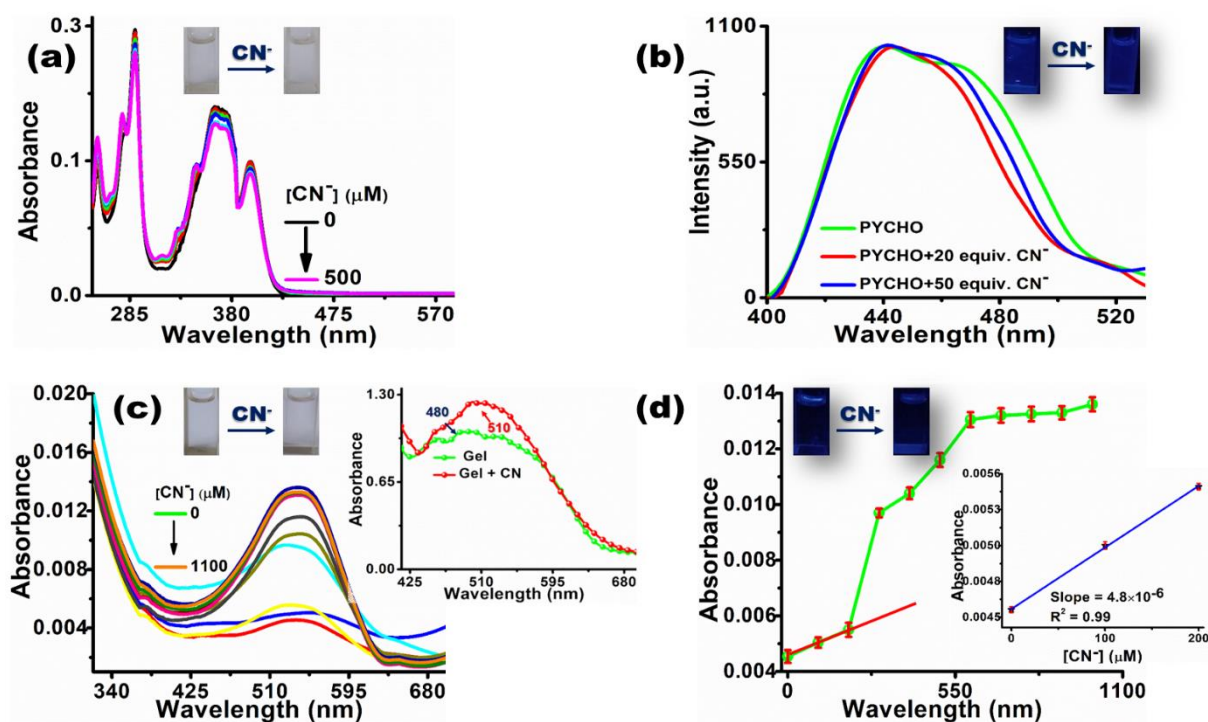
Fig. S45 (a) Variations in UV/Vis absorption and (b) emission spectral responses (λ_{ex} = 370 nm) of PYCHO (concentration = 10 μM) along with monitored solution colors observed under day (Inset of Fig. S45a) and UV light (Inset of Fig. S45b) in presence of added [CN⁻] in 8:2 (v/v) DMSO/water. (c) Changes in UV/Vis absorption spectra of 4-ACN (Concentration = 10 μM) along with monitored solution color (Inset of Fig. S45c) in presence of added [CN⁻] in 8:2 (v/v) DMSO/water. Inset of Fig S45c also indicates change in UV/Vis absorption spectrum of CN1 gel before and after CN⁻ addition. (d) Variation in absorbance (λ_a = 540 nm) and its linear response (Inset Fig. S45d) with respect to added [CN⁻] in 8:2 (v/v) DMSO/water along with UV-photograph of 4-ACN before and after CN⁻ addition

Table S10 Quantitative analysis (DLs) of sensory response from PYCHO, CN1 and 4-ACN towards CN⁻

Detection limits (DLs)		
PYCHO*	CN1	4-ACN
-	0.48 ± 0.01 μM (gel) 5.42 ± 0.256 nM (solution)	62.08 ± 0.09 μM (solution)

* Due to unaltered UV/Vis absorption and/or fluorescence spectral responses, DLs could not be calculated
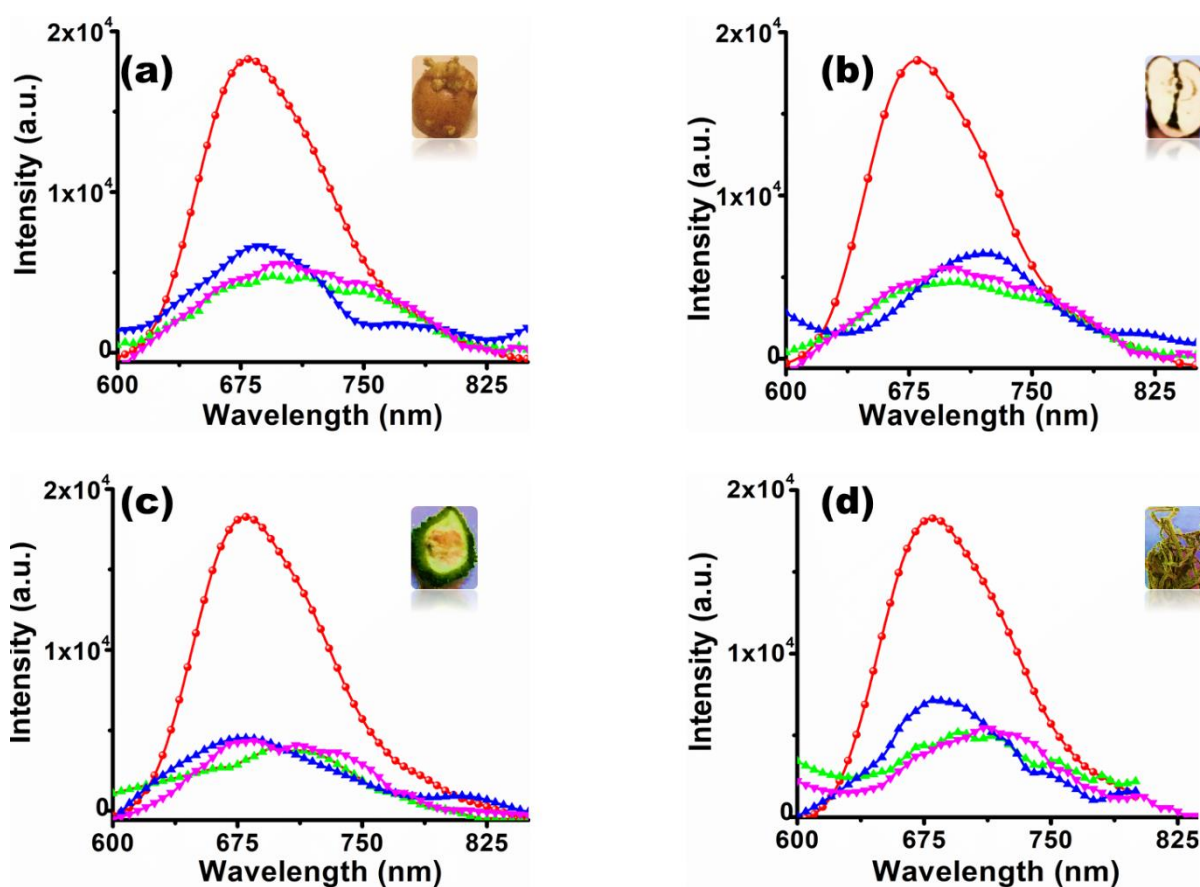
Fig. S46 Quantitative estimation of CN⁻ from (a) sprouted potato, (b) apple seeds, (c) bitter seeds and (d) Sudan grasses based on fluorogenic quenching response of 8:2 (v/v) DMSO/water gel (1 wt%) ($\lambda_{ex} = 450$ nm).

References

1 N. P. B. Hoi and B. Eckert, *Recuell des Travaux Chimiques des Pays-Bas et de la Belgique*, 1955, **74**, 1119–1124.

2 R. Y. Lin, C. Lee, Y. Chen, J. Peng, T. C. Chou, H. Yang, J. T. Lina and K. Ho, *Chem. Commun.*, 2012, **48**, 12071–12073.

3 Y. Kawamura, H. Sasabe and C. Adachi, *Jpn. J. Appl. Phys.*, 2004, **43**, 7729–7730.

4 A. Adhikary, K. S. Das, S. Saha, M. Roy and R. Mondal, *Dalton Trans.*, 2020, **49**, 13487–13495.

5 L. Zhai, Y. Shu, J. Sun, M. Sun, Y. Song and R. Lu, *Eur. J. Org. Chem.*, 2019, **2019**, 3093–3100.

6 M. J. Frisch, G. W. Trucks, H. B. Schlegel, G. E. Scuseria, M. A. Robb, J. R. Cheeseman, G. Scalmani, V. Barone, B. Mennucci, G. A. Petersson, H. Nakatsuji, M. Caricato, X. Li, H. P. Hratchian, A. F. Izmaylov, J. Bloino, G. Zheng, J. L. Sonnenberg, M. Hada, M. Ehara, K. Toyota, R. Fukuda, J. Hasegawa, M. Ishida, T. Nakajima, Y. Honda, O. Kitao, H. Nakai, T. Vreven, J. A. Montgomery Jr, J. E. Peralta, F. Ogliaro, M. Bearpark, J. J. Heyd, E. Brothers, K. N. Kudin, V. N. Staroverov, R. Kobayashi, J. Normand, K. Raghavachari, A. Rendell, J. C. Burant, S. S. Iyengar, J. Tomasi, M. Cossi, N. Rega, J. M. Millam, M. Klene, J. E. Knox, J. B. Cross, V. Bakken, C. Adamo, J. Jaramillo, R. Gomperts, R. E. Stratmann, O. Yazyev, A. J. Austin, R. Cammi, C. Pomelli, J. W. Ochterski, R. L. Martin, K. Morokuma, V. G. Zakrzewski, G. A. Voth, P. Salvador, J. J. Dannenberg, S. Dapprich, A. D. Daniels, O. Farkas, J. B. Foresman, J. V. Ortiz, J. Cioslowski and D. J. Fox, Gaussian 09, Revision D.01, Gaussian Inc., Wallingford, CT, 2009.

7 Y. Xu, P. Xue, D. Xu, X. Zhang, X. Liu, H. Zhou, J. Jia, X. Yang, F. Wanga and R. Lu, *Org. Biomol. Chem.*, 2010, **8**, 4289–4296.

8 C. Long, J. -H. Hu, P. -W. Ni, Z. -y. Yin and Q. -Q. Fu, *New J. Chem.*, 2018, **42**, 17056–17061.

9 T. Sun, Q. Niu, Y. Li, T. Li, T. Hu, E. Wang and H. Liu, *Sens. Actuators B Chem.*, 2018, **258**, 64–71.

10 R. Kaushik, A. Ghosh, A. Singh, P. Gupta, A. Mittal and D. A. Jose, *ACS Sens.*, 2016, **1**, 1265−1271.

11 S. Pramanik, V. Bhalla and M. Kumar, *ACS Appl. Mater. Interfaces*, 2014, **6**, 5930−5939.

12 L. Yang, X. Li, J. Yang, Y. Qu and J. Hua, *ACS Appl. Mater. Interfaces*, 2013, **5**, 1317−1326.

13 X. Cheng, Y. Zhou, J. Qin and Z. Li, *ACS Appl. Mater. Interfaces*, 2012, **4**, 2133−2138.

14 X. Cheng, R. Tang, H. Jia, J. Feng, J. Qin and Z. Li, *ACS Appl. Mater. Interfaces*, 2012, **4**, 4387−4392.

15 Z. M. Dong, H. Ren, J. N. Wang and Y. Wang, *Microchem. J.*, 2020, **155**, 104676.

16 M. H. Chua, H. Zhou, T. T. Lin, J. Wu and J. Xu, *J. Mater. Chem. C*, 2017, **5**, 12194−12203.

17 S. Dey, C. Sen and C. Sinha, *Spectrochim. Acta A*, 2020, **225**, 117471.

18 E. Ramachandran, S. A. A. Vandarkuzhali, G. Sivaraman and R. Dhamodharan, *Chem. Eur. J.*, 2018, **24**, 11042–11050.

19 A. Panja and K. Ghosh, *ChemistrySelect*, 2018, **3**, 1809–1814.

20 J. Li, W. Wei, X. Qi, G. Zuo, J. Fang and W. Dong, *Sens. Actuators B Chem.*, 2016, **228**, 330–334.

21 J. Li, X. Qi, W. Wei, Y. Liu, X. Xu, Q. Lin and W. Dong, *Sens. Actuators B Chem.*, 2015, **220**, 986–991.

22 I. J. Kim, M. Ramalingam and Y. -A. Son, *Sens. Actuators B Chem.*, 2017, **246**, 319–326.

23 C. Yang, X. Wang, Z. Xu and M. Wang, *Sens. Actuators B Chem.*, 2017, **245**, 845–852.

24 T. Ghosh, S. Mitra, S. K. Maity and D. K. Maiti, *ACS Appl. Nano Mater.*, 2020, **3**, 3951−3959.

25 P. R. Lakshmi, R. Manivannan, P. Jayasudha and K. P. Elango, *Anal. Methods*, 2018, **10**, 2368–2375.

26 J. Jin, J. Zhang, L. Zou and H. Tian, *Analyst*, 2013, **138**, 1641–1644.

27 S. Suganya, E. Ravindran, M. K. Mahato and E. Prasad, *Sens. Actuators B Chem.*, 2019, **291**, 426–432.

28 S. Manickam and S. K. Iyer, *RSC Adv.*, 2020, **10**, 11791–11799.

29 S. Sharma, M. Kumari and N. Singh, *Soft Matter*, 2020, **16**, 6532−6538.

30 A. Sebastian and E. Prasad, *Langmuir*, 2020, **36**, 10537−10547.

31 F. Mandegani, H. Zali-Boeini, Z. Khayat and R. Scopelliti, *Talanta*, 2020, **219**, 121237.

32 C. Nandhini, P. S. Kumar, K. Poongodi, R. Shanmugapriya and K. P. Elango, *J. Mol. Liq.*, 2021, **327**, 114833.

33 H. Yao, J. Wang, S. -S. Song, Y. -Q. Fan, X. -W. Guan, Q. Zhou, T. -B. Wei, Q. Lin and Y. -M. Zhang, *New J. Chem.*, 2018, **42**, 18059–18065.

34 N. Malviya, M. Das, P. Mandal and S. Mukhopadhyay, *Soft Matter*, 2017, **13**, 6243–6249.

35 Q. Niu, L. Lan, T. Li, Z. Guo, T. Jiang, Z. Zhao, Z. Feng and J. Xi, *Sens. Actuators B Chem.*, 2018, **276**, 13–22.